J. Fluid Mech. (1990), *vol.* 218, *pp.* 405–438
Printed in Great Britain

Experimental support for the attached-eddy hypothesis in zero-pressure-gradient turbulent boundary layers

By A. E. PERRY AND J. D. LI
Department of Mechanical and Manufacturing Engineering, University of Melbourne, Parkville, Victoria 3052, Australia

(Received 14 August 1989 and in revised form 10 February 1990)

Turbulent boundary layer experiments have been conducted at various Reynolds numbers on smooth walls and also on 'k-type' and 'd-type' rough walls. Both the spectral results and the broadband turbulence intensity results strongly support the Townsend (1976) attached eddy hypothesis and the Perry & Chong (1982) model. The spectral results obtained using the 'flying' hot-wire technique show the errors involved when using Taylor's (1938) hypothesis for converting the spectra from the frequency domain to the wavenumber domain. If the viscous dissipation spectral region is taken into account, the broadband turbulence intensity results agree well with the attached eddy hypothesis. The inconsistency of the various constants given in Perry, Lim & Henbest (1987) for the smooth and rough walls has been explained and removed. Lack of spatial resolution of the hot wires explains to some extent the scatter in the turbulence intensity of the component normal to the wall. This spatial resolution effect is most pronounced in the near-wall region at high Reynolds number and has been corrected by using the method of Wyngaard (1968).

1. Introduction

In recent work by Perry, Lim & Henbest (1987), the turbulence structure in zero-pressure-gradient boundary layers above smooth and rough surfaces was investigated in the light of Townsend's (1976) attached-eddy hypothesis, the theories of Perry & Chong (1982), Perry, Henbest & Chong (1986) and the extension of the dimensional analysis approaches of Perry & Abell (1977). Encouraging support for these hypotheses and theories was found but because of hot-wire anemometry difficulties there were inconsistencies in some of the comparisons between smooth and rough surfaces. Also, the proposed similarity laws for the component of velocity fluctuations normal to the wall were inconclusive because of considerable scatter in the results of many workers. Furthermore, there were uncertainties in the inferred wavenumbers when using Taylor's hypothesis for converting the spectra from the frequency domain to the wavenumber domain, particularly at low wavenumbers. These problems are addressed in this paper and attention is focused on the turbulent wall region (where the mean flow follows a logarithmic distribution) of zero-pressure-gradient turbulent boundary layers over smooth walls and also over 'k-type' and 'd-type' rough walls.

2. Similarity laws and some recent extensions and development

The coordinate system used here will be x for the streamwise direction, y for the lateral direction and z for the distance normal to the wall. U is the streamwise mean velocity, u_1, u_2 and u_3 the streamwise, lateral and normal to the wall velocity fluctuations respectively and U_1 is the free-stream velocity.

According to the dimensional analysis approach of Perry *et al.* (1986), the one-dimensional power spectral density $\phi_{11}(k_1)$ of the u_1 velocity fluctuations in the fully turbulent wall region has three identifiable ranges of the streamwise wavenumber k_1. These are an outer-flow scaling at low wavenumbers, an inner-flow scaling from low to moderate wavenumbers and a Kolmogorov scaling at moderate to high wavenumbers.

A region of overlap between the outer-flow scaling and the inner-flow scaling is found to exist (overlap region I) which leads to

$$\frac{\phi_{11}(k_1\delta_H)}{U_\tau^2} = \frac{A_1}{k_1\delta_H} \quad \text{or} \quad \frac{\phi_{11}(k_1 z)}{U_\tau^2} = \frac{A_1}{k_1 z} \tag{1}$$

where the argument of ϕ_{11} gives the unit quantity over which the spectral density is measured, U_τ the wall friction velocity, and δ_H is the boundary-layer thickness, which is the value of z from the wall to the edge of the boundary layer. The precise definition is given in the Appendix. The thickness δ_H is close to Δ_E used by Perry *et al.* (1987). One can see that an overlap is possible only if an inverse power law is valid and the constant A_1 is universal.

At high wavenumbers a second region of overlap appears to occur between the 'inner-flow' scaling region and the Kolmogorov region (overlap region II) and it is found that

$$\frac{\phi_{11}(k_1 z)}{U_\tau^2} = \frac{K_0}{\kappa^{\frac{2}{3}}}\frac{1}{(k_1 z)^{\frac{5}{3}}} \quad \text{or} \quad \frac{\phi_{11}(k_1\eta)}{v^2} = \frac{K_0}{(k_1\eta)^{\frac{5}{3}}}, \tag{2}$$

where $\eta = (\nu^3/\epsilon)^{\frac{1}{4}}$ is the Kolmogorov lengthscale, $v = (\nu\epsilon)^{\frac{1}{4}}$ is the Kolmogorov velocity scale, K_0 is a universal constant, κ is the Kármán constant (throughout this paper it is taken to be 0.41) and ϵ is the local energy dissipation rate. It can be seen that such an overlap is possible only if the famous $-\frac{5}{3}$ power law of Kolmogorov (1941) is valid (the inertial subrange). In deriving (2), Townsend's assumption for the turbulent wall region has been used, i.e. local energy production is closely in balance with local energy dissipation. It should be pointed out that the $-\frac{5}{3}$ power-law spectra are observed at wavenumbers far below those needed for an inertial subrange to exist according to the classical method of approach. Perhaps at the low-wavenumber end of the $-\frac{5}{3}$ power law observed here the eddies are not isotropic but the degree of isotropy increases with increasing wavenumbers. Also, as Reynolds number increases, the length of the $-\frac{5}{3}$ law increases and so also does the range of wavenumbers where motions are isotropic. An identical analysis can be carried out for the spanwise fluctuation spectrum $\phi_{22}(k_1)$ except that A_1 is replaced in (1) by a different universal constant A_2 and the condition of isotropy from equation (12) given later means that in the inertial subrange $\phi_{22}(k_1)$ with (2) is given by $\phi_{22}(k_1) = \frac{4}{3}\phi_{11}(k_1)$.

These relationships are consistent with the picture of wall turbulence as put forward by Perry *et al.* (1986) which follows. The inverse power law in the spectrum is consistent with the ideas that the mean vorticity and Reynolds shear stress as well as most of the energy-containing motions are contributed by coherent attached eddies (possibly of horseshoe, Λ or Π shapes). A random array of such eddies which are at various stages of stretching constitutes a so-called 'hierarchy', and there is present a range of geometrically similar hierarchies, the lengthscales of which follow an inverse power law p.d.f., i.e. $P_H(\delta) \sim 1/\delta$. The hierarchies are assumed to have a constant velocity scale U_τ. This gives a logarithmic mean velocity profile, a finite Reynolds shear stress at the wall ($z/\delta_H \to 0$) in the turbulent wall region at infinite Reynolds number as well as an inverse-power-law spectral region for ϕ_{11}. On a smooth wall the scale δ varies from $\delta_1 \approx 100\nu/U_\tau$ (the smallest hierarchy) to the

boundary-layer thickness δ_H, which scales with the largest hierarchy. Here δ could be thought of as the height of a representative eddy within a given hierarchy. On a 'k-type' rough wall the smallest hierarchy scale is assumed to be proportional to the roughness scale k. On a 'd-type' rough wall, it is conjectured that both the smallest and largest hierarchies scale with δ_H, giving a fixed fractional spread in hierarchy lengthscales. Surrounding these attached motions are incoherent statistically isotropic motions which contribute to the Kolmogorov region and are responsible for the energy dissipation but are thought not to contribute greatly to the mean vorticity or Reynolds shear stress.

For the normal spectrum ϕ_{33}, Perry *et al.* (1986) argued, using the attached-eddy hypothesis, that the only eddies which contribute significantly scale with the distance z from the wall. Thus there is no outer-flow scaling and only one overlap region exists, which is the inertial subrange, and a factor of $\frac{4}{3}$ must be introduced in this region, i.e. with (2), $\phi_{33}(k_1) = \frac{4}{3}\phi_{11}(k_1)$.

The inconvenience of the above spectral scaling laws is that they are not given by a single formula valid over the entire wavenumber range. Perry *et al.* (1988*a*) derived such formulae from a curve fitting procedure for each component. Although there is no physical basis for these more general formulae, they are designed to give a fairly accurate indication of the shape of the spectra while preserving the asymptotic laws such as the -1 law and the $-\frac{5}{3}$ law with all the correct scalings.

The spectrum formula for the streamwise velocity component which incorporates these scaling laws is

$$\frac{\phi_{11}(k_1\delta_H)}{U_\tau^2} = \frac{A'}{G_1 G_2}, \tag{3}$$

where

$$G_1 = \{1+[\tfrac{1}{2}\{1+\tanh(\theta(k_1\delta_H - q))\}\alpha k_1 \delta_H]^2\}^{\frac{1}{2}},$$

$$G_2 = \left\{1+\left[\beta\frac{U_\tau^2}{\upsilon^2}A'\frac{1}{(k_1\eta)K_{11}(k_1\eta)}\right]^m\right\}^{1/m},$$

with constants $A' = 2.06$, $\alpha = 2.0$, $\beta = 0.72$, $\theta = 2$, $q = 0.78$ and $m = 3$.

The normal component spectrum is

$$\frac{\phi_{33}(k_1 z)}{U_\tau^2} = \frac{B'}{\left\{1+\left[\beta\frac{U_\tau^2}{\upsilon^2}\left(\frac{z}{\eta}\right)\frac{1}{K_{33}(k_1\eta)}\right]^m\right\}^{1/m}}, \tag{4}$$

where $B' = 0.9$, $m = 0.5$ and $\beta = 0.9$.

The various constants in (3) and (4) are chosen according to the data from Perry *et al.* (1987) and the data to be discussed here. According to Perry *et al.* (1988*a*) 'they are subject to alteration without notice' and in fact already have been given updated values here.

The terms $K_{11}(k_1\eta)$ and $K_{33}(k_1\eta)$ in (3) and (4) are the one-dimensional spectra derived by using Kovasznay's (1948) spectral expression in the Kolmogorov equilibrium region. They are

$$K_{11}(k_1\eta) = \begin{cases} 0.500(k_1\eta)^{-\frac{5}{3}} - 6.04(k_1\eta)^{-\frac{1}{3}} - 1.8(k_1\eta) + 0.306(k_1\eta)^2 + 7.03 & \text{for } k_1\eta \leqslant 1.22, \\ 0 & \text{for } k_1\eta > 1.22, \end{cases} \tag{5}$$

and

$$K_{33}(k_1\eta) = \begin{cases} 0.669(k_1\eta)^{-\frac{5}{3}} - 4.02(k_1\eta)^{-\frac{1}{3}} - 0.153(k_1\eta)^2 + 3.51 & \text{for } k_1\eta \leqslant 1.22, \\ 0 & \text{for } k_1\eta > 1.22. \end{cases} \tag{6}$$

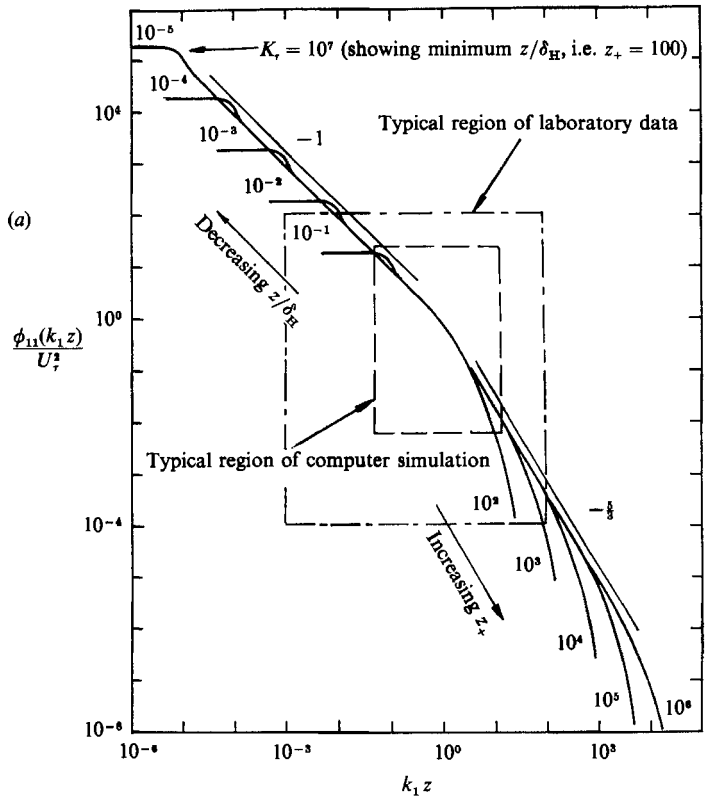

FIGURE 1(*a*). For caption see facing page.

Figures 1(*a*) and 2(*a*) show the maximum wavenumber range that direct simulations on present day supercomputers are capable of producing, compared with the laboratory data range and the meteorological range. It can be seen that the -1 law and the $-\frac{5}{3}$ law are very pronounced only when K_τ approaches 10^6. Here $K_\tau = \delta_H U_\tau/\nu$, the Kármán number, and this high value is reached only for meteorological data.

Figures 1(*b*) and 2(*b*) show the pre-multiplied forms of the spectra plotted semi-logarithmically so that the area under these graphs is proportional to the spectral energy. The low-wavenumber 'bump' is obvious in the $\phi_{11}(k_1)$ spectrum. This 'bump' is thought to represent the contribution of energy in the wall region from large-scale eddies $\delta \approx O(\delta_H)$ which also contribute to the Coles (1956) wake function. Perry *et al.* (1986) and Perry (1987) argued that the inverse power law p.d.f. of hierarchy scales needs to be weighted by a weighting function that is larger than unity for $\delta \approx O(\delta_H)$ to account for this extra energy from the large-scale eddies. In fact, in the model discussed by Perry *et al.* (1986), the contribution to the power spectral density from attached eddies was shown to be given by the convolution integral (see their equation (26))

$$\frac{k_1 z \phi_{11}(k_1 z)}{U_\tau^2} \propto \int_{\lambda_1}^{\lambda_E} \frac{\psi_{11}(\alpha, \lambda)}{U_\tau^2} w(\lambda - \lambda_E)|_{k_1 z = \text{const.}}\, d\lambda, \tag{7}$$

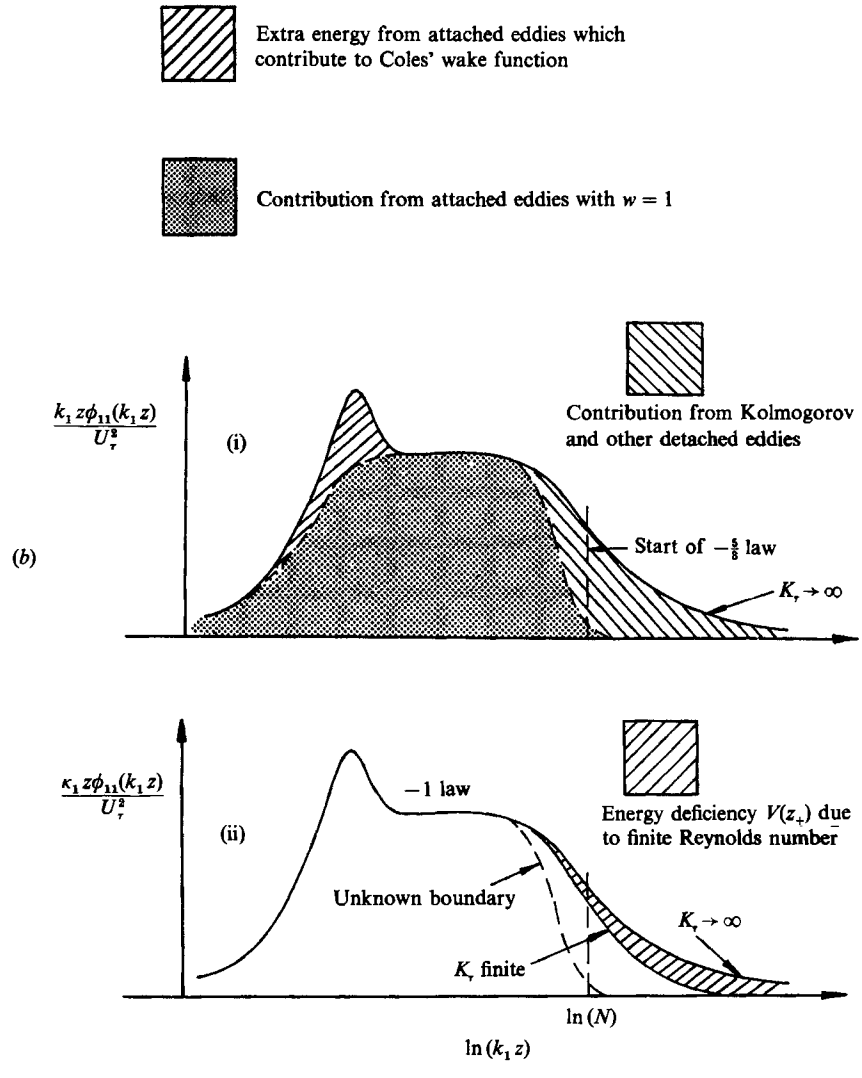

FIGURE 1. (*a*) The u_1 spectra in the turbulent wall region generated using equation (3). (*b*) Pre-multiplied u_1 spectra: (i) energy contribution from $K_\tau \to \infty$; (ii) finite-Reynolds-number case.

where $\psi_{11}(\alpha, \lambda)$ is the universal pre-multiplied spectral density calculated from a hierarchy of scale δ, $\lambda = \ln(\delta/z)$, $\lambda_1 = \ln(\delta_1/z)$, $\lambda_E = \ln(\delta_H/z)$, $\alpha = \ln(k_1\delta)$ and w is the weighting function which can be expressed as a function of δ/δ_H. It is assumed that all hierarchies are geometrically similar and that motions contributed by one hierarchy are uncorrelated with those of another and so spectral contributions can be added linearly. This assumption appears to be working, from the data given here and other wall data referred to. It is expected that this weighting function would depend on the large-scale geometry and the flow situation, i.e. it would depend on whether we have turbulent wall flow in a circular pipe, a rectangular duct, a zero-pressure-gradient boundary layer or an adverse-pressure-gradient boundary layer.

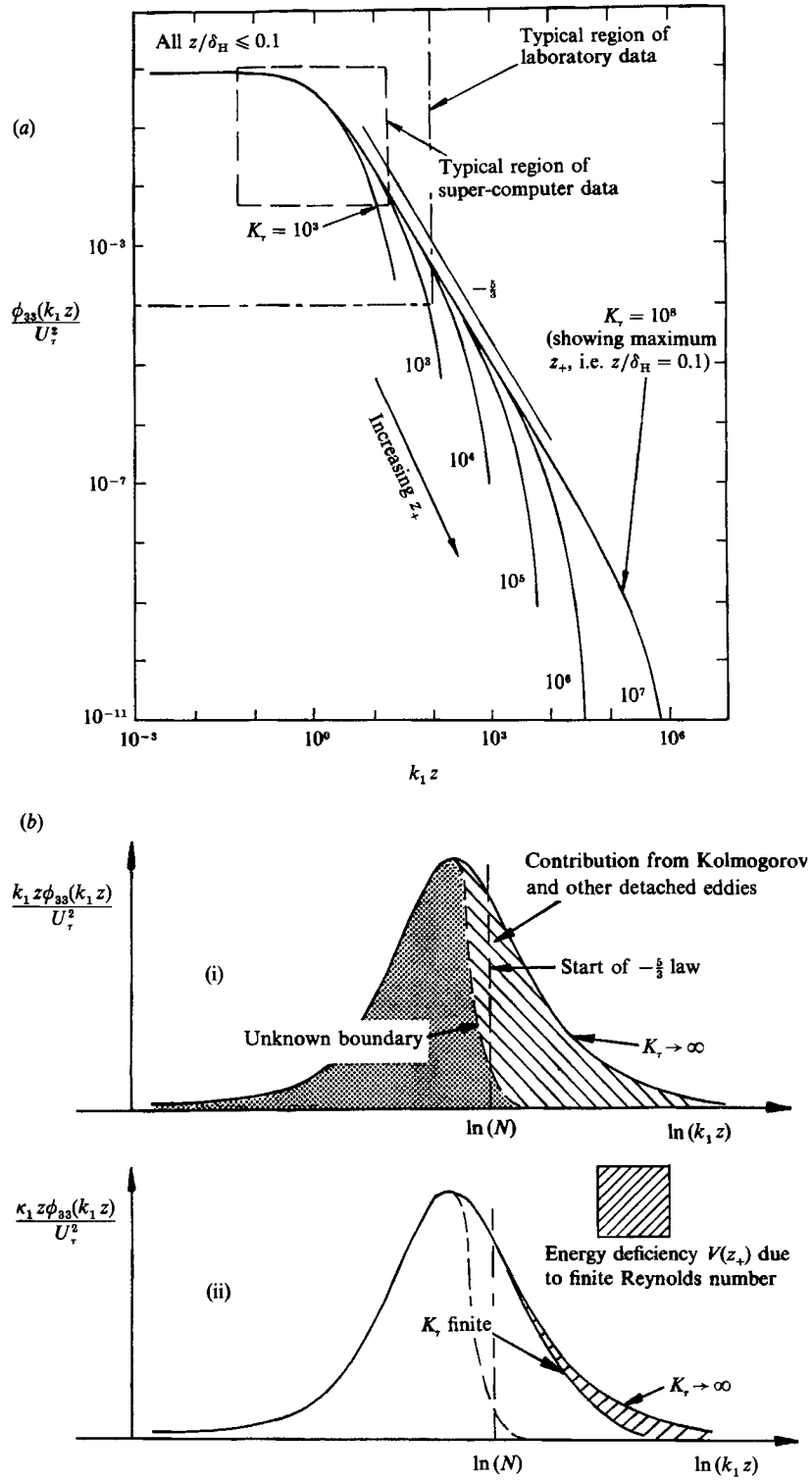

FIGURE 2. (*a*) The u_3 spectra in the turbulent wall region generated using equation (4). (*b*) Pre-multiplied u_3 spectra: (i) energy contribution from $K_\tau \to \infty$; (ii) finite-Reynolds-number case.

In fact, this weighting function and hence the low-wavenumber bump will probably depend on Coles' wake factor Π in the equation

$$\frac{U}{U_\tau} = \frac{1}{\kappa}\ln\frac{zU_\tau}{\nu} + A - \frac{\Delta U}{U_\tau} + \frac{\Pi}{\kappa}\xi\left(\frac{z}{\delta_c}\right), \tag{8}$$

where A is a universal constant ($= 5.0$), ξ the Coles wake function, δ_c the Coles boundary-layer thickness, which is related to δ_H, and $\Delta U/U_\tau$ is the Hama (1954) roughness function. With $w = 1$, it is expected that $\Pi = 0$ and there would be no low-wavenumber bump. However, for $\delta/\delta_H = O(1)$, w is larger than unity and the bump is present.

Perry, Li & Marušić (1988*b*), Perry *et al.* (1988*a*) and Li (1989) have developed these ideas further and have proposed an attached-eddy model with weighting functions which enables the theory to be applied to adverse-pressure-gradient boundary layers with some success, and work along these lines is continuing.

By integrating the spectrum over the whole wavenumber region, after neglecting the contribution from the region beyond the overlap region II, Perry *et al.* (1986) expressed the u_1-broadband turbulence intensity in the turbulent wall region as

$$\frac{\overline{u_1^2}}{U_\tau^2} = B_1 - A_1\ln\frac{z}{\delta_H} - C(z_+)^{-\frac{1}{2}}, \tag{9}$$

where C is a universal constant, B_1 a large-scale characteristic constant and $z_+ = zU_\tau/\nu$. Figure 3 is a plot of (3) in pre-multiplied form for $K_\tau \to \infty -$ or $z_+ \to \infty$ for different values of z/δ_H. This figure shows schematically the contribution to $\overline{u_1^2}$ from different regions of the spectrum and explains why B_1 and B_2 (below) are characteristic constants. The figure also shows that the -1 power law increases as z/δ_H decreases. By using a similar analysis, Perry *et al.* (1986) obtained the broadband turbulence intensity profiles for the other two components as

$$\frac{\overline{u_2^2}}{U_\tau^2} = B_2 - A_2\ln\frac{z}{\delta_H} - \tfrac{4}{3}C(z_+)^{-\frac{1}{2}}, \tag{10}$$

$$\frac{\overline{u_3^2}}{U_\tau^2} = A_3 - \tfrac{4}{3}C(z_+)^{-\frac{1}{2}}, \tag{11}$$

where A_2 and A_3 are universal constants and B_2 is a large-scale characteristic constant. The factor $\frac{4}{3}$ in (10) and (11) comes from the isotropic condition for the spectra in the Kolmogorov region. The turbulent wall region has been tentatively defined by Perry *et al.* (1987) as being $z_+ \geqslant 100$; $z/\delta_H < 0.15$.

Perry *et al.* (1987) attempted to verify the broadband turbulence intensity formulae (9), (10) and (11) for turbulent boundary layers over smooth and rough walls. They found that the broadband turbulence intensities for the streamwise and the spanwise components agree reasonably well with (9) and (10). For the component normal to the wall, the results were inconclusive. They attributed this to errors in the hot-wire anemometry techniques used and found that the data from other workers also gave inconclusive results.

Spalart (1988) has pointed out that the factor $\frac{4}{3}$ in (10) and (11) should not be present, and the viscous correction term in (9), (10) and (11) should be isotropic because it has been assumed that the flow is isotropic in the Kolmogorov region. When deriving the broadband turbulence intensity by integrating the spectra, it has recently been found that the rather crude approximation of neglecting the energy beyond the region of overlap II, i.e. for $k_1\eta > 0.085$ (the dissipation region) is inadequate for laboratory Reynolds numbers, particularly for the $\overline{u_3^2}$ component.

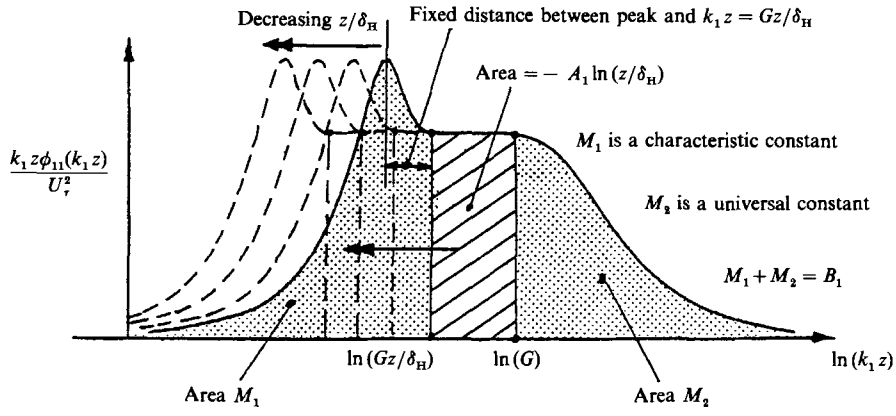

FIGURE 3. Graphic representation of terms in equation (3) for $K_\tau \to \infty$. G is a universal constant appropriately chosen so that $k_1 z = G$ and $k_1 z = G(z/\delta_H)$ fall in the -1 region.

Also, for isotropic flow the following relationship exists (Batchelor 1953 or Hinze 1975) for one-dimensional spectra:

$$\phi_{33}(k_1) = \phi_{22}(k_1) = \frac{1}{2}\left\{\phi_{11}(k_1) - k_1 \frac{\mathrm{d}\phi_{11}(k_1)}{\mathrm{d}k_1}\right\}. \tag{12}$$

Equation (12) shows that the sudden arbitrary cutoff of the $\phi_{11}(k_1)$ at the high-wavenumber end introduces a Dirac delta function if we want isotropy for $\phi_{22}(k_1)$ and $\phi_{33}(k_1)$. This delta function was erroneously excluded in the Perry *et al.* (1986) analysis and with its inclusion the factor $\frac{4}{3}$ in (10) and (11) becomes unity.

Instead of neglecting the viscous-affected region, the full power spectral density expressions in (5) and (6) were used in Perry *et al.* (1988*a*) and Li (1989) in the equilibrium region for isotropic flow. Because the flow in the turbulent boundary layer is not isotropic for all wavenumbers, this spectral expression can be applied only beyond some wavenumber. In the turbulent wall region, this is $k_1 z = N$ according to Perry *et al.* (1986), where N is a universal constant. Here again, a cutoff problem has been introduced with associated delta functions for the u_2 and u_3 components, this time at the lower wavenumber end ($k_1 z = N$). To avoid this difficulty, the viscous correction term in the streamwise direction only has been derived and we shall keep in mind that the viscous correction is isotropic, i.e. it is the same for all three components. Thus the broadband turbulence intensities with viscous correction are (Perry *et al.* 1988*a* and Li 1989)

$$\frac{\overline{u_1^2}}{U_\tau^2} = B_1 - A_1 \ln\left(\frac{z}{\delta_H}\right) - V(z_+), \tag{13}$$

$$\frac{\overline{u_2^2}}{U_\tau^2} = B_2 - A_2 \ln\left(\frac{z}{\delta_H}\right) - V(z_+), \tag{14}$$

$$\frac{\overline{u_3^2}}{U_\tau^2} = A_3 - V(z_+). \tag{15}$$

Spalart (1988), by fitting his supercomputer data, obtained

$$V(z_+) = 4.37(z_+)^{-\frac{1}{2}}. \tag{16}$$

If Kovasznay's (1948) formula is used to fit the spectra in the Kolmogorov equilibrium region, i.e. for $k_1 z > N$, it can be shown that

$$V(z_+) = 5.58(z_+)^{-\frac{1}{2}} - 22.4(z_+)^{-1} + 22.0(z_+)^{-\frac{5}{4}} - 5.62(z_+)^{-2} + 1.27(z_+)^{-\frac{11}{4}}. \tag{17}$$

This has the same function form as (16) when z_+ becomes large. At $z_+ = 100$, equation (17) gives $V(z_+) = 0.403$ while (16) gives 0.437.

One of the consequences of (13)–(15) is that there is no 'law of the wall' for $\overline{u_1^2}/U_\tau^2$ or $\overline{u_2^2}/U_\tau^2$ for $z_+ \geqslant 100$; $z/\delta_H < 0.15$, but there should be one for $\overline{u_3^2}/U_\tau^2$. Recent results of Wei & Willmarth (1989) (their figure 15) give encouraging support for this. The only departure is the lowest Reynolds number $\overline{u_3^2}/U_\tau^2$, where $K_\tau \approx 200$ is too low for a fully turbulent wall region to exist and the two points closest to the wall for the highest Reynolds number for $\overline{u_3^2}/U_\tau^2$ appear to fall outside the trends indicated by other data in the figure.

Equations (13)–(17) and further developments based on these are compared with experimental results in §4.

3. Experimental apparatus and methods

3.1. *Wind tunnel and hot-wire anemometry*

The wind tunnel including the 'flying' hot-wire facility are basically the same as described in Perry *et al.* (1987). The *k*-type roughness is a wire mesh and was fixed on the wall and the mesh is identical to that of Perry *et al.* (1987). The *d*-type roughness was an array of narrow spanwise grooves. In fact it is the same aluminium plate with machined grooves as used by Perry, Schofield & Joubert (1969). Grooves were 3 mm wide, 3 mm deep and 5.7 mm pitch†, and spanned the working section of 910 mm width. The working section height is 410 mm and is about 4 m long.

The essential difference between the two types of roughness are that for *k*-type roughness $\Delta U/U_\tau$ in (8) depends on kU_τ/ν and roughness element geometry where k is the roughness scale, and for *d*-type roughness $\Delta U/U_\tau$ depends only on $\delta_H U_\tau/\nu$ and roughness geometry.

All the hot-wire measurements with normal and ×-wires were taken using platinum Wollaston wires, with a 5 μm diameter and 1 mm length and separation. Different lengths and separations were used only when checking hot-wire behaviour. The effect of the wire length and separation was taken into account by using the spatial resolution correction method given by Wyngaard (1968). For the ×-wires, the wire angles to the free-stream direction are nominally ±45° to the mean velocity direction and on a few occasions ±60° angle wires were used in order to check the cone angle problem (Perry *et al.* 1987) and for the measurement of the Reynolds shear stress on rough walls. An increase in the relative velocity between fluid and wires produced by 'flying' the probe in the upstream direction reduces the cone angle of velocity vectors relative to the wires. Constant-temperature hot-wire anemometers were used throughout the experiments and the details of the electronic circuit and calibration procedure are close to those given in Perry (1982). A resistance ratio of 2 was used unless otherwise specified. Signals were sampled on-line by a PDP 11/10 digital computer using a 12-bit A-D converter. The calibration and measuring procedures used analogue voltage sums and differences from ×-wires and the wires were electronically matched so that for small perturbations, voltage waveforms are proportional to velocity waveforms. The calibration procedure, however, accounts for the nonlinear response of the wires.

A normal wire was used to measure the streamwise spectrum and the ±45° ×-wire probe was used to measure the u_2 and u_3 spectra. A fast Fourier transform algorithm was applied to the voltage waveforms and it has been shown (Li 1989) that this gives

† Spacing was incorrectly reported in Perry *et al.* (1969) (a decimal point error).

almost identical results for the waveforms converted to velocities using the nonlinear hot-wire calibration. Voltage waveforms were therefore used for measuring spectra because of the more rapid data processing.

The spectral argument was converted from the frequency f to the one-dimensional longitudinal wavenumber k_1 using Taylor's (1938) hypothesis, which assumes that the eddying motions are frozen in time relative to an observer moving with the local mean velocity. Many workers have questioned the validity of this hypothesis, among them Lin (1952), Wills (1964) and Zaman & Hussain (1981). Section 5.1 includes an investigation of this hypothesis using the flying-hot-wire system. All spectra have been normalized using the following relationships:

$$\overline{u_1^2} = \int_0^\infty \phi_{11}(k_1)\,\mathrm{d}k_1, \quad \overline{u_2^2} = \int_0^\infty \phi_{22}(k_1)\,\mathrm{d}k_1, \quad \overline{u_3^2} = \int_0^\infty \phi_{33}(k_1)\,\mathrm{d}k_1. \tag{18}$$

3.2. *Wall shear velocity*

For smooth walls, the Clauser chart (Clauser 1954) and the Preston-tube methods (Patel 1965) were used to obtain the skin friction and it was found that they agree very well (to within 1.5%) for U_τ values. In general, the values obtained from the Preston-tube method were smaller. In this paper, all the turbulence results on smooth walls were non-dimensionalized using the wall shear velocity obtained from the Preston-tube method.

There is no easy way to find the skin friction coefficient on rough walls. For smooth walls, the Clauser-chart method includes only one unknown $U_\tau/U_1 = (\frac{1}{2}C_f')^{\frac{1}{2}}$, where C_f' is the local skin friction coefficient. As Perry & Joubert (1963) have pointed out. three unknowns are presented on rough walls, namely, the 'error in origin' e, the roughness function $\Delta U/U_\tau$, and U_τ/U_1. Here e is the distance below the crest of the element from where z should be measured to give a logarithmic mean velocity profile.

Various schemes have been derived to determine the above parameters for rough walls. These schemes rely either on the Hama (1954) velocity defect law, e.g. Perry *et al.* (1987) and Bandyopadhyay (1987) or Coles' (1956) law of the wall and law of the wake function, e.g. Tani (1987). The problem with the above methods is that they all put too much weight on the properties of the outer part of the layer and hence rely too heavily on having a universal defect law. This is equivalent to having a constant value of the wake factor Π in the Coles formula (8).

On rough walls, the error in origin contaminates the mean flow data near the wall (causing them to depart from the logarithmic law) and the upstream history causes the non-dimensional defect plot to vary from station to station (small differences in Π) in zero-pressure-gradient boundary layers. What is needed is a method that is insensitive to Π. Based on this motivation, the following method for determining the U_τ values on rough walls is proposed.

From (8) with $\Pi = 0.55$, it can be shown that the mean velocity in the logarithmic wall region is given as

$$\frac{U}{U_1} = 1 + \frac{1}{\kappa}\frac{U_\tau}{U_1}\ln\frac{z}{\delta^*} + \frac{1}{\kappa}\frac{U_\tau}{U_1}\ln\frac{U_\tau}{U_1} + 0.493\frac{U_\tau}{U_1}, \tag{19}$$

where δ^* is the displacement thickness of the boundary layer. By plotting U/U_1 versus z/δ^*, a family of curves similar to a Clauser chart can be obtained with different U_τ/U_1 values. Figure 4 shows the procedure. First assume $e = 0$, i.e. z is measured from the crest of the element, and plot the data as shown in figure 4. The data points that are close to but below $z/\delta^* = 1$ are used and compared with the

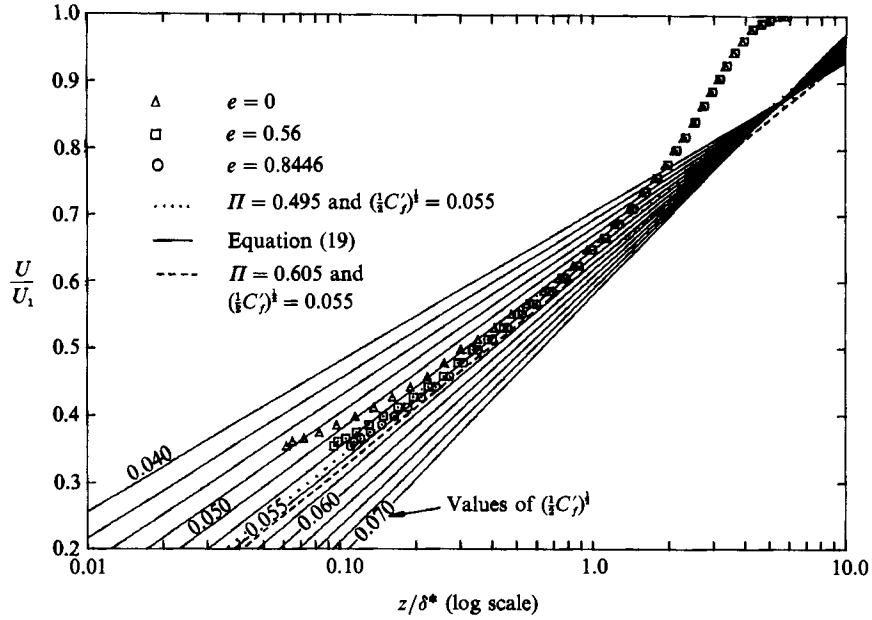

FIGURE 4. The method for determining the skin friction over a rough wall.

constant-U_τ/U_1 lines. Thus a first estimated value of U_τ/U_1 can be found. From the data near the wall, i.e. $z/\delta^* \ll 1$, a first estimated error in origin value can be found. This error in origin is then added to the distance from crest of the elements and this results in more data points following the logarithmic line. Thus the second set of U_τ/U_1 and e values can be obtained. After two or three iterations, the values for U_τ/U_1 and e converge. Testing of this method shows that a $\pm 10\%$ variation in the value of Π will cause only a $\pm 3\%$ variation in the inferred values of U_τ/U_1. This method will be referred to as the 'modified Clauser method'.

Two other methods have been used for determining the value of U_τ/U_1. One is the momentum integral method which requires the mean flow to be very closely two-dimensional. Another makes use of the measured Reynolds shear stress profiles. This also requires two-dimensionality and analytical expressions for the Reynolds shear stresses in the form of

$$\frac{-\overline{u_1 u_3}}{U_\tau^2} = f\left(\frac{z}{\delta_H}, \frac{U_\tau}{U_1}, K_\tau, \Pi\right). \tag{20}$$

These can be derived from the mean momentum and continuity equations together with (8). Π can be assumed approximately constant with x for rough walls and for smooth walls Π is related to Reynolds number (e.g. see Coles 1962). An iteration method can easily be devised using data and the above formula for determining U_τ. Preliminary work on this method was reported by Li, Henbest & Perry (1986) and a more complete analysis has been carried out by Li & Perry (1989).

All these of the above methods have been applied to both the k-type and d-type rough walls and they agree with each other to within $\pm 3\%$ for U_τ. This is surprising, particularly for the momentum integral method. However, the experimental set-up was carefully tested by Lim (1985) for two-dimensionality by taking spanwise traverses of the mean spanwise component of velocity to ensure that no secondary flow was present. As a matter of interest, the same good agreement was found for the smooth-wall results using the above three methods. Because not all these methods

were used for all profiles, the U_τ values from the modified Clauser chart method were used for the k-type roughness and the Reynolds shear stress method was used for the d-type roughness.

3.3. *Spatial resolution correction and the broadband turbulence intensity measurement*

Hot-wire measurements can resolve only those eddies that have the same or larger lengthscales than the hot-wire length used. Uberoi & Kovasznay (1953), Wyngaard (1968), Bremhorst (1972) and Roberts (1973) have investigated this spatial filtering problem theoretically under various assumptions. In order to avoid this spatial resolution problem, some workers have been developing subminiature hot-wire probes, see Willmarth & Bogar (1977), Willmarth & Sharma (1984), Ligrani & Bradshaw (1987*a*, *b*), Nakayama & Westphal (1986) and Ligrani, Westphal & Lemos (1989). In the work here, Wyngaard's (1968) method was used. His formulae were applied to the measured spectral results to determine the missing energy caused by the lack of spatial resolution. This missing energy was then added to the broadband turbulence intensity results. In cases where it was thought to be necessary, for example on smooth walls at high Reynolds numbers, a small amount of energy due to low-pass filters being set at 10 kHz was calculated using the spectral formulation of Kovasznay and added to the broadband results.

For $\overline{u_1^2}/U_\tau^2$ measurements, the spatial resolution problem was not serious. Typically, at $z/\delta_H = 0.1$, $\overline{u_1^2}/U_\tau^2 \approx 5$, $\overline{u_2^2}/U_\tau^2 \approx 2$, while $\overline{u_3^2}/U_\tau^2 \approx 1$. It turns out that the absolute errors (i.e. the energy deficiencies) caused by the lack of spatial resolution is approximately the same for all three components if local isotropy at high wavenumbers is valid. However, because of the difference in magnitude of the three components as indicated above, the fractional errors are quite different. For instance, a 20% error for $\overline{u_3^2}/U_\tau^2$ (one of the largest errors) corresponds to only 4% error for $\overline{u_1^2}/U_\tau^2$. This is within our experimental error for turbulence measurements and so no corrections were made to $\overline{u_1^2}/U_\tau^2$, but they were made to $\overline{u_3^2}/U_\tau^2$ in the turbulent wall region.

4. Broadband turbulence intensities

Mean flow, broadband turbulence intensities and spectral measurements were undertaken for smooth walls, k-type and d-type rough walls for different Kármán numbers. Tables 1(*a*) and 1(*b*) show the cases measured. In the present work, the mean flow for smooth walls was tripped in such a way as to produce a wake factor Π which follows as closely as possible to the curve suggested by Coles (1962). Figure 5 shows the measured Π distribution for different flow cases.

4.1. *Longitudinal turbulence intensity*

Figure 6 shows the longitudinal turbulence intensities measured using stationary normal wires. It can be seen that the results collapse very well in the outer part of the boundary layer and show some Reynolds-number dependence in the turbulent wall region, although there is some scatter. This Reynolds-number dependence can be explained using the spectral scaling laws given by Perry *et al.* (1986). Also plotted in figure 6 are the theoretical curves from (13) for the corresponding lowest and highest Kármán numbers of the experimental data as well as for the infinite Reynolds-number case. The constant A_1 is obtained from the spectral results and B_1 is obtained from the best curve fit to the experimental results plotted in figure 6. In the present results, $A_1 = 1.03$ and $B_1 = 2.39$. The $V(z_+)$ term in (13) has been

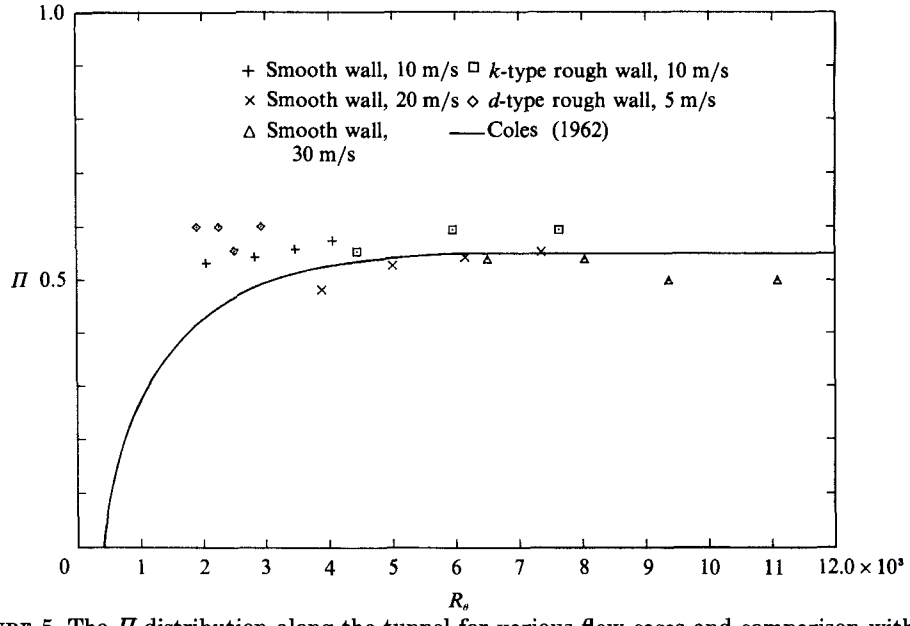

FIGURE 5. The Π-distribution along the tunnel for various flow cases and comparison with the data of Coles (1962).

		x (mm)	U_1 (m/s)	R_θ	K_τ
(*a*)		1780	10	2828	1193
		2400	10	3471	1473
		3030	10	4066	1681
		1780	20	5008	2106
		2400	20	6152	2534
		3030	20	7357	3000
		1780	30	8045	3313
		2400	30	9371	3780
		3030	30	11097	4433
(*b*)	*k*-type	2100	10	5970	2755
		2800	10	7645	3498
	d-type	2060	5	2243	985
		2460	5	2497	1086

TABLE 1. (*a*) Smooth-wall flow parameters; (*b*) rough-wall flow parameters

calculated by two different methods. One uses the expression given by (17), shown by the dashed lines in figure 6. It can be seen that the curves fit the data reasonably well but the spread of the calculated curves is less than the experimental data in the turbulent wall region. It was felt that the reason for this might be because expression (17) was obtained using Kovasznay's (1948) formula beyond the non-dimensional wavenumber $k_1 z = N = 2.5$ according to the suggestion of Perry *et al.* (1987). It is suspected that at this wavenumber, which Perry *et al.* considered to be the start of the $-\frac{5}{3}$ law, the Kovasznay formula does not match up with the experimental spectrum in the turbulent boundary layer at finite Reynolds number, but that this difference vanishes as the Reynolds number increases. The second method uses the

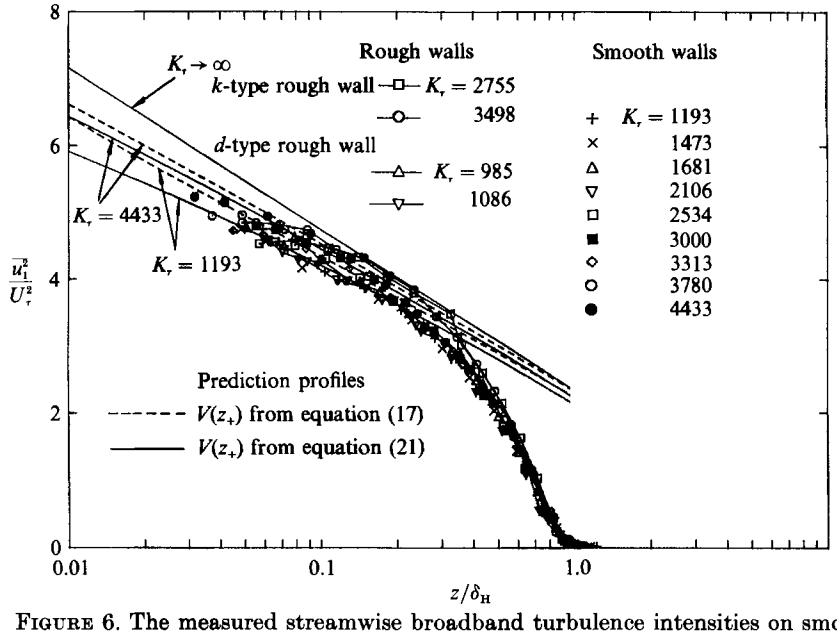

FIGURE 6. The measured streamwise broadband turbulence intensities on smooth and rough walls.

curve-fitted spectra expression as given by (3). By expressing v and η in terms of U_τ and z, $V(z_+)$ can be expressed as

$$V(z_+) = \operatorname*{Lim}_{z_+ \to \infty} \left\{ \int_0^\infty \frac{A'}{G_1 G_2} \mathrm{d}(k_1 \delta_H) \right\} - \int_0^\infty \frac{A'}{G_1 G_2} \mathrm{d}(k_1 \delta_H). \tag{21}$$

Although at high wavenumbers we are still using the Kovasznay formula, the expression is continuous in the whole wavenumber range and fits the spectral data well in the regions of most concern (Perry *et al.* 1988*a*). Figure 7 shows diagrammatically the various different methods for obtaining $V(z_+)$ including the earlier 'sudden cutoff' method. In figure 6, the solid lines are calculated from (13) with $V(z_+)$ calculated using (21). It can be seen that this shows the best agreement with the data. Hence,

$$\frac{\overline{u_1^2}}{U_\tau^2} = 2.39 - 1.03 \ln\left(\frac{z}{\delta_H}\right) - V(z_+). \tag{22}$$

In figure 6, the k-type rough wall results show some slightly higher values than the smooth-wall results. An explanation for this is the difference in the wake factor Π. Figure 5 shows that the Π values on the k-type and d-type rough walls are about 0.6, while on the smooth wall they almost follow the Coles' curve.

Perry *et al.* (1987) have given two different sets of constants. On smooth walls, they obtained $A_1 = 1.03$ and $B_1 = 2.48$ and on k-type rough walls, $A_1 = 1.26$ and $B_1 = 2.01$. Spalart (1988), by fitting his direct supercomputer simulation results (on a smooth wall), gave $A_1 = 1.1$ and $B_1 = 2.0$. According to the spectral scaling laws, the constant A_1 should be universal, i.e. the same for smooth and rough walls. The only difference between the smooth and rough walls from the point of view of the Perry & Chong (1982) model is that the smallest hierarchy scales with ν/U_τ on smooth walls while it scales with the roughness scale on rough walls. The present results in figure 6 show that the constant A_1 is the same on both the smooth and rough walls and this

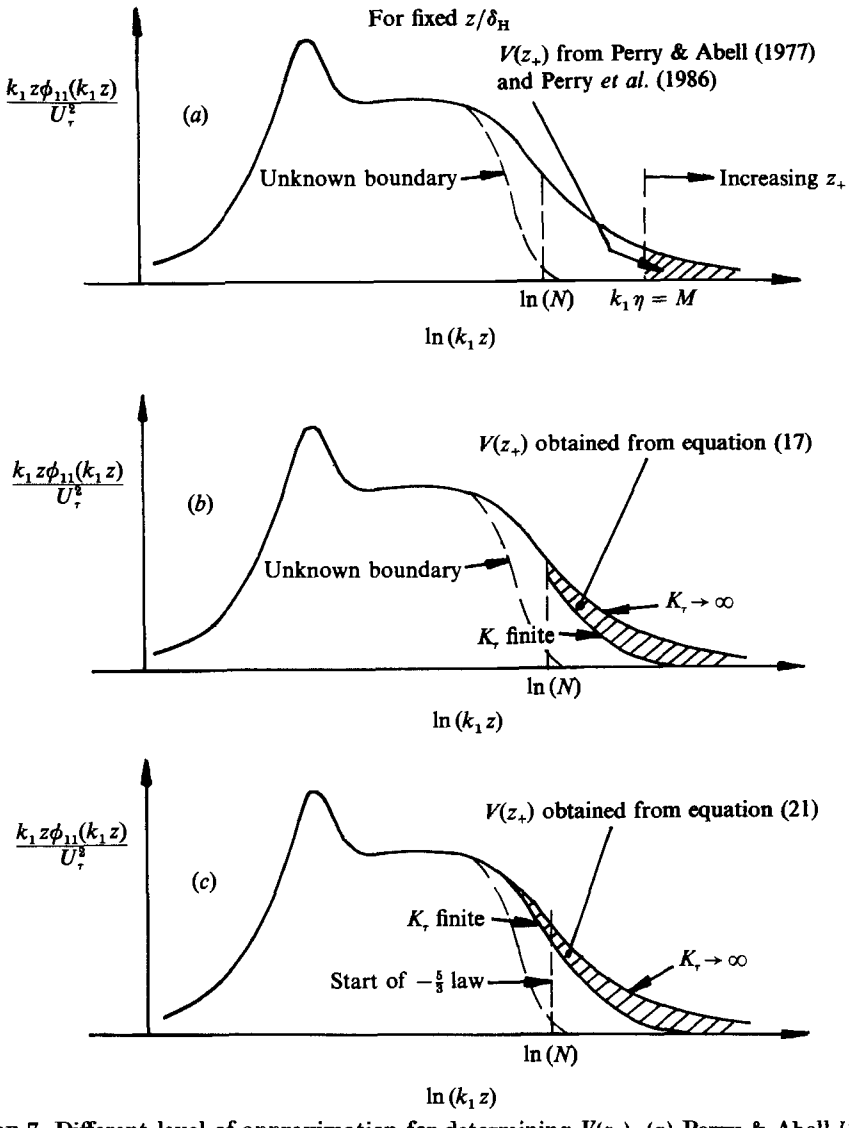

FIGURE 7. Different level of approximation for determining $V(z_+)$. (*a*) Perry & Abell (1977) and Perry *et al.* (1986); (*b*) equation (17); (*c*) equation (21).

also agrees reasonably well with Spalart's result. The difference in A_1 between the smooth and rough walls in Perry *et al.* (1987) might be due to the different modified Clauser-chart method used for determining the wall shear velocity U_τ on their k-type rough walls, i.e. as mentioned earlier, too much weighting being given to the outer flow.

4.2. *Lateral turbulence intensity*

Figure 8 shows the lateral turbulence intensities measured by using the calibrated $\times$-wires. Li (1989) has shown that the maximum cone angle in the (U, V)-Plane is about 20° for the range of smooth-wall measurements made. According to Perry *et al.* (1983) stationary $\times$-wires set at $\pm 45°$ should not suffer a serious cone angle problem when the maximum cone angle is less than 20°. The lateral turbulence intensities have been measured only for the smooth walls. The results have been corrected for spatial

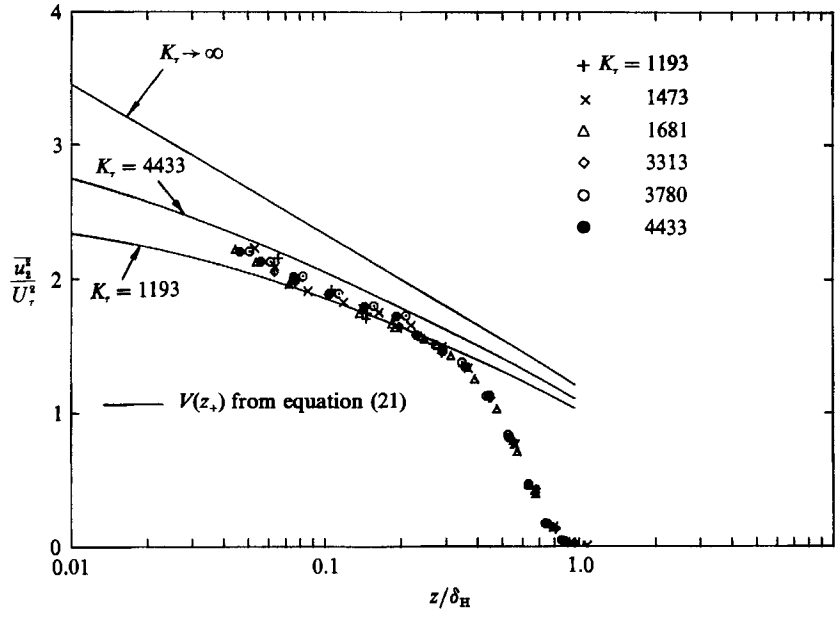

FIGURE 8. The measured spanwise broadband turbulence intensities on smooth walls with the spatial resolution correction applied.

resolution effects for points within the turbulent wall region. For the results outside the wall region, spatial resolution corrections have not been applied since they were found to be negligible. Also plotted in figure 8 are the calculated curves obtained using the following equation:

$$\frac{\overline{u_2^2}}{U_\tau^2} = 1.20 - 0.475 \ln\left(\frac{z}{\delta_H}\right) - V(z_+), \tag{23}$$

where $A_2 = 0.475$ is found from the spectral data (given later) and $B_2 = 1.20$ is found from the best curve fit of the above formula to the experimental data. Following the same argument as in §4.1, $V(z_+)$ has been calculated from (21). It is the same as for the streamwise component since this part of the correction should be closely isotropic. It can be seen that the data agree well with (23).

The spectral scaling laws show that the constant A_2 should be a universal constant. The present results give $A_2 = 0.475$ while Perry *et al.* (1987) gave $A_2 = 0.73$ on smooth walls and $A_2 = 0.63$ on rough walls and Spalart (1988) gave $A_2 = 0.66$. However, a re-check of the spectral data from Perry *et al.* (1987) indicates $A_2 = 0.55$ on smooth walls and $A_2 = 0.50$ on rough walls. Spalart's data (1988, figure 17) indicate that he relied too heavily on his data between $z/\delta_H = 0.2 \sim 0.3$ which is outside the turbulent wall region. Judging from all these factors, it seems that A_2 should have a value of about 0.5 for both the smooth and rough walls. This agrees reasonably well with the present result.

4.3. *Normal turbulence intensity*

If we assume that $\overline{u_3^2} = f(z, \nu, U_\tau, \delta_H)$ in turbulence pipe and duct flows, a simple dimensional analysis using the Buckingham π theorem shows that

$$\frac{\overline{u_3^2}}{U_\tau^2} = \phi\left(\frac{z}{\delta_H}, K_\tau\right). \tag{24}$$

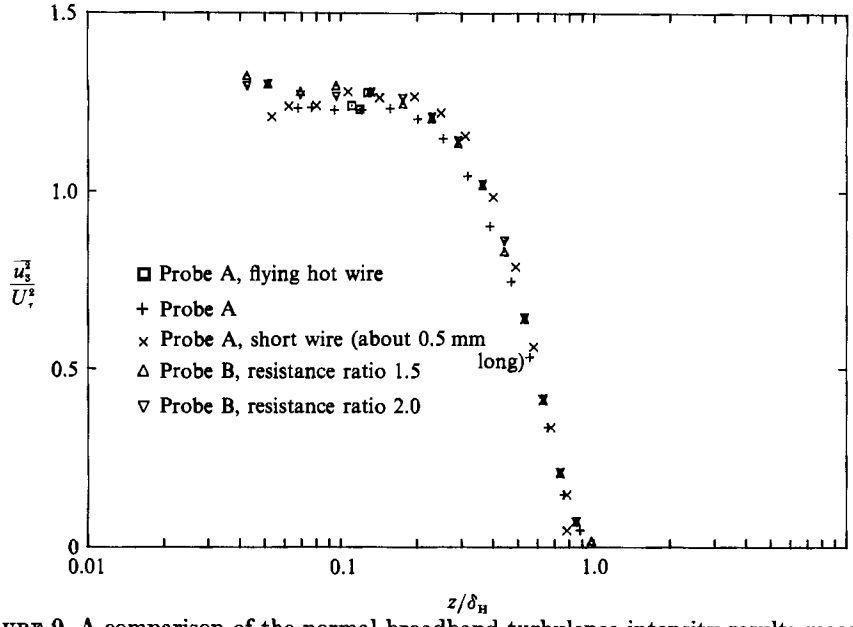

FIGURE 9. A comparison of the normal broadband turbulence intensity results measured using probe A and B with different wires and under different operating conditions shown.

In zero-pressure-gradient turbulent boundary layers, because the streamwise development is slow, the above result should also be applicable. Equation (24) shows that u_3^2/U_τ^2 at $z/\delta_H = 0.1$ *vs.* K_τ should collapse on a universal curve, but the experimental data from world-wide sources are very disappointing, as shown in Perry *et al.* (1987), who attributed the enormous scatter of $\pm 50\%$ to poor hot-wire anemometry practice and suggested that spatial resolution might be one of the problems. When performing turbulence measurements using hot wires, some problems that could explain these discrepancies are: (i) thermal prong effects, which affect the frequency response of the wire (see Perry, Smits & Chong 1979); (ii) hot-wire filament bowing (Perry 1982); (iii) probe misalignment; (iv) excessive cone angles of the approaching velocity vectors (see Perry *et al.* 1983, 1987); (v) aerodynamic prong effects and (vi) the spatial resolution effect.

Some of the problems have been checked respectively by (i) operating the same set of ×-wires at different resistance ratios; (ii) using different sets of ×-wires and checking the hot-wire filament bowing; (iii) checking for probe misalignment; (iv) Perry *et al.* (1987) have shown that near the wall on smooth walls, the cone angles are small; and (iv) using two different probe–prong geometries. Figure 9 shows the results from such checks at a free-stream velocity of 10 m/s on the smooth wall. It can be seen that the results collapse very well at the same Reynolds number. Perry *et al.* (1987) show the results of a similar test (their figure 22) where the same good collapse did not occur. In figure 9, probe A is the probe most commonly used and has a configuration similar to the DISA 55P51 while probe B is a smaller probe with a configuration similar to DISA 55P61.

In figure 10, the measured normal broadband turbulence intensity results are shown where the smooth-wall data have been corrected for spatial resolution effects and low-pass filter roll-off while the flying hot-wire results have been used in the turbulent wall region for the k-type rough wall to avoid the excessive cone angle

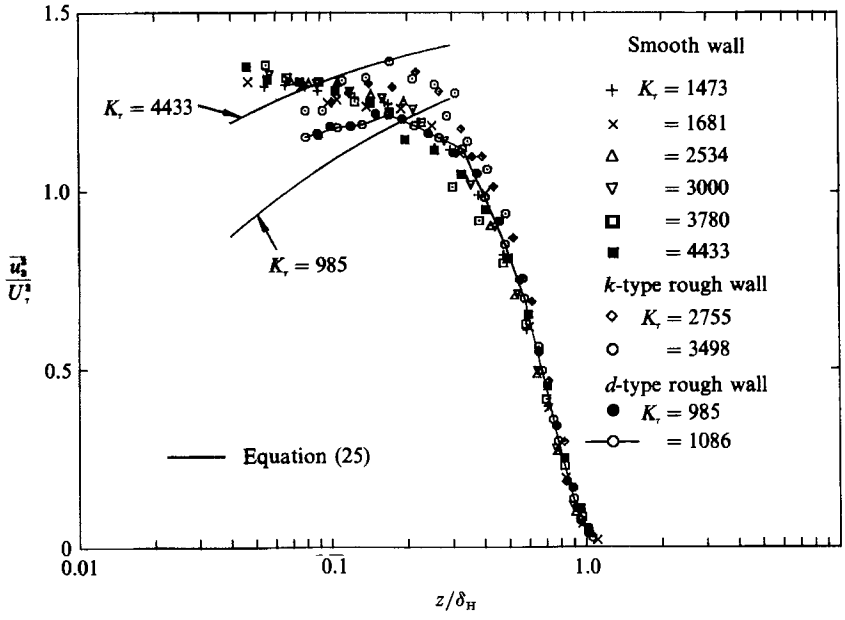

FIGURE 10. The measured normal broadband turbulence intensities with the spatial resolution correction applied to the smooth-wall results. (In the turbulent wall region, the flying-hot-wire results have been used for k-type rough-wall data.)

problem with × -wires. Also shown in figure 10 are the calculated curves from $z/\delta_H = 0.04$ to 0.3 from (15) with $A_3 = 1.6$ and $V(z_+)$ calculated from (21).

The results for the d-type and the k-type rough walls have not been corrected for the spatial resolution effect. This is because on the d-type rough wall, the Kármán number is low and it is found at this low Kármán number, the corrections are negligible. On the k-type rough wall, only the flying wire results can be trusted because a stationary $\pm 45°$ wire suffers a cone angle problem and the $\pm 60°$ wire results are not reliable for $\overline{u_3^2}$ measurements. Experience has shown that at a free-stream velocity of 10 m/s, the spatial resolution and the low-pass filter roll-off corrections are small on smooth walls. It is felt that at a free-stream velocity of 10 m/s on k-type rough walls, this should also be true. (The spectral results also show that the k-type rough wall spectra at a free-stream velocity of 10 m/s are close to the smooth-wall spectra at about the same free-stream velocity.)

Figure 11 shows $\overline{u_3^2}/U_\tau^2$ at $z/\delta_H = 0.1$ *vs.* K_r for the results from the present experiments as well as some data from other workers. Much of the data in Perry *et al.* (1987) have not been selected because we have set the following criteria in choosing the data: (i) if spatial resolution corrections are necessary then we require the accompanying spectra so as to apply the Wyngaard (1968) correction; (ii) if cone angle problems are seen to be a difficulty, e.g. over k-type rough surfaces, then we use only flying-hot-wire data; and (iii) over smooth walls, if the measured Reynolds shear stress using × -wires, after being extrapolated to the wall, shows inconsistencies with the U_τ^2 values obtained from the Clauser-chart or Preston-tube methods then we reject the data. Also plotted in figure 11 are the calculated curves with $V(z_+)$ given by various equations. It can be seen that the data and the solid curve agree best. Here $V(z_+)$ is given by (21) and the best fit for (15) gives $A_3 = 1.6$, i.e.

$$\frac{\overline{u_3^2}}{U_\tau^2} = 1.6 - V(z_+). \tag{25}$$

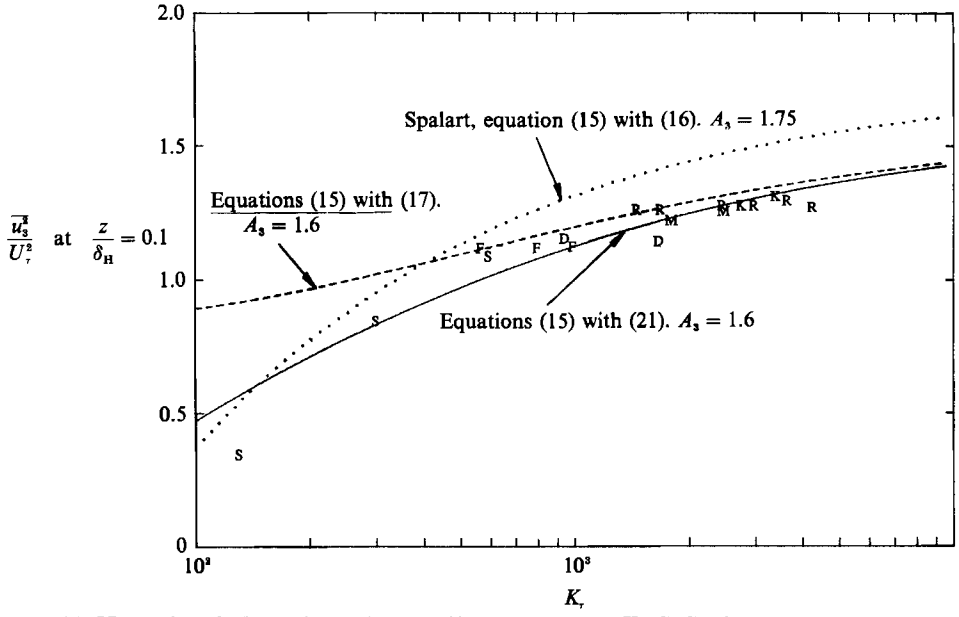

FIGURE 11. Normal turbulence intensity at $z/\delta_H = 0.1$ versus K_τ. S, Spalart (1988) supercomputer simulation; D, d-type rough wall; F, Erm, Smith & Joubert (1986) low Reynolds number; K, k-type rough wall, flying wire result (spatial resolution effect for D, F and K is small); R, present smooth-wall results, spatial resolution effect has been corrected, M, Ligrani *et al.* (1989 and also private communication), subminiature hot wire. Theoretical curves shown.

The two lowest Reynolds-number results from Spalart (1988) should strictly not be included since $z/\delta_H = 0.1$ finishes up in the buffer zone. Also the authors suspect that the calculated values for $V(z_+)$ shown in figure 11 become inaccurate for K_τ less than 500. A dotted curve representing equation (16) given by Spalart (1988) is shown in figure 11 with his recommended $A_3 = 1.75$. It can be seen that this curve is higher than most of the experimental results.

The three curves shown in figure 11 represent the three different levels of approximation shown earlier in figure 7. These should have the same functional form for z_+ sufficiently large, i.e. $V(z_+) \to C(z_+)^{-\frac{1}{2}}$, where C is a universal constant, but have different functional forms for low z_+. Equation (21) seems the most satisfactory but it should be kept in mind that this was derived from (3) and (5) which to some extent are arbitrary.

5. Turbulence spectra and the convection velocity problem

The spectral results over smooth and k-type rough walls are presented. Perry *et al.* (1987) have already presented an extensive set of results and only new findings will be emphasized.

5.1. *Streamwise-component spectra in the turbulent wall region*

Figures 12, 13, and 14 show all the streamwise spectra measured with normal wires over smooth walls and k-type rough walls, plotted using inner-flow scaling, Kolmogorov scaling and outer-flow scaling respectively. Throughout this paper the Kolmogorov scales were calculated assuming that energy production is equal to energy dissipation. The collapse to the various scaling laws is reasonable except that there appears to be an excessive spread at low wavenumbers for spectra with outer-

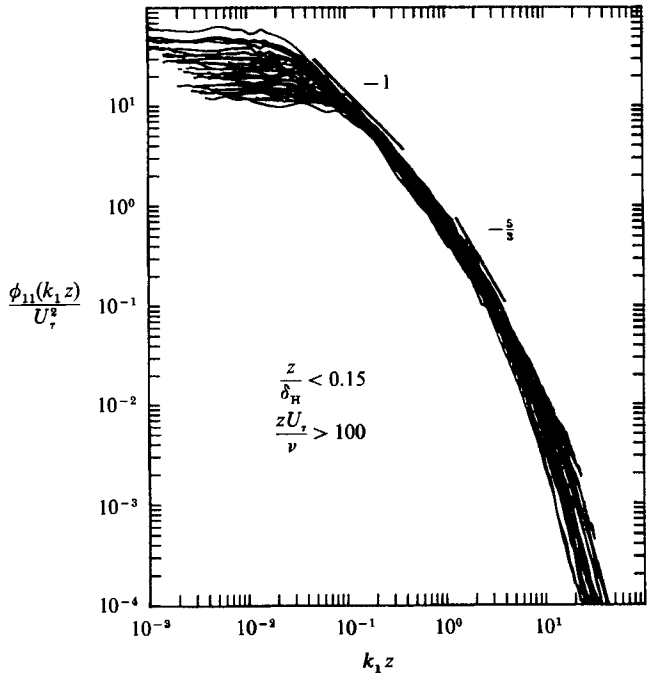

FIGURE 12. Longitudinal spectra in the turbulent wall region, inner-flow scaling.

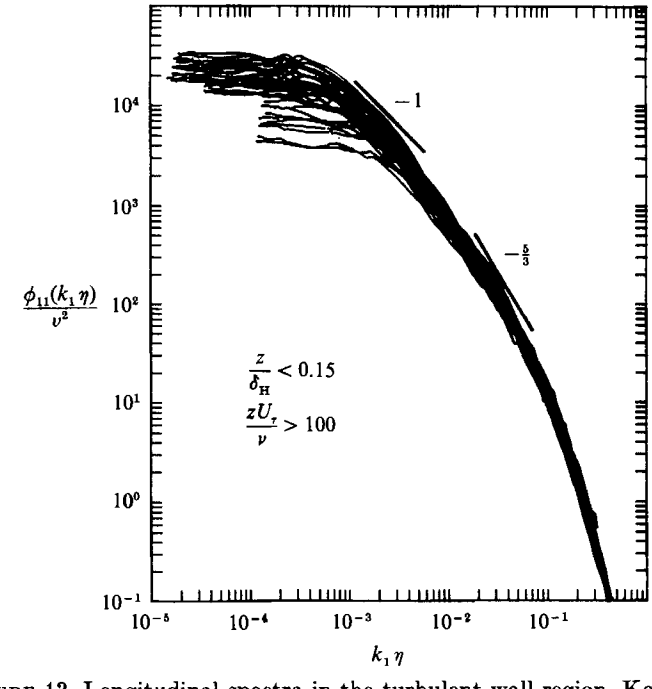

FIGURE 13. Longitudinal spectra in the turbulent wall region, Kolmogorov scaling.

flow scaling. It has been suggested by Perry *et al.* (1986) that this lack of collapse of data at low $k_1 \delta_H$ (as in figure 14) may be due to the invalid use of Taylor's (1938) hypothesis for inferring wavenumbers k_1 from frequency f using $k_1 = U/2\pi f$, where U is local mean velocity at a fixed point and this is assumed to be the convection

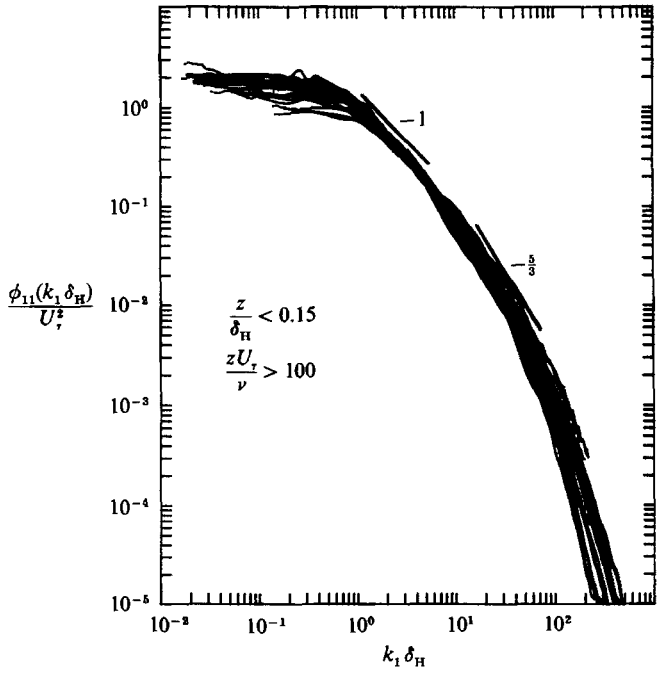

FIGURE 14. Longitudinal spectra in the turbulent wall region, outer-flow scaling.

velocity for eddies of all scales whose influence passes this fixed point. It is suspected that the larger scale coherent attached eddies are convected downstream at some faster rate than the smaller scale eddies and hence there is a spread in convection velocity for a given wavenumber as suggested by Wills (1964) for flow in jets. Perry *et al.* (1986) carried out a crude simulation for estimating the convection velocity effect on spectra by assuming that attached eddies in a hierarchy of scale δ are convected at the local mean velocity at $z = \frac{1}{2}\delta$. Figure 15 shows the results of this simulation and explains the lack of collapse at low wavenumber in figure 14.

A spectral function which illustrates quite graphically that not only is there a spread in convection velocity with given wavenumber but also there exist a spread in wavenumbers for a given convection velocity has been given by Wills (1964) following the suggestion of Ffowcs Williams. This function is

$$W(k,c) = \frac{1}{(2\pi)^2}\int_{-\infty}^{\infty}\int_{-\infty}^{\infty}\overline{u_1^2}R(r,\tau)\,\mathrm{e}^{\mathrm{i}k(r-c\tau)}\,\mathrm{d}r\,\mathrm{d}\tau, \tag{26}$$

where $W(k,c)$ is the energy per unit wavenumber interval and per unit convection velocity interval. Here c is the convection (or phase) velocity, $R(r,\tau)$ is the two-point space–time correlation coefficient, r is the streamwise spacing between two points in the flow and τ is a time shift between the two points.

Perry & Abell (1977) pointed out that the relationship between the function $W_0(k,c)$ measured by an observer in laboratory coordinates and the function $W_u(k,c)$ measured by an observer moving at velocity U is given by

$$W_u(k,c) = W_0(k,c-U). \tag{27}$$

This means that the $W(k,c)$ contours translate without distortion for a change in

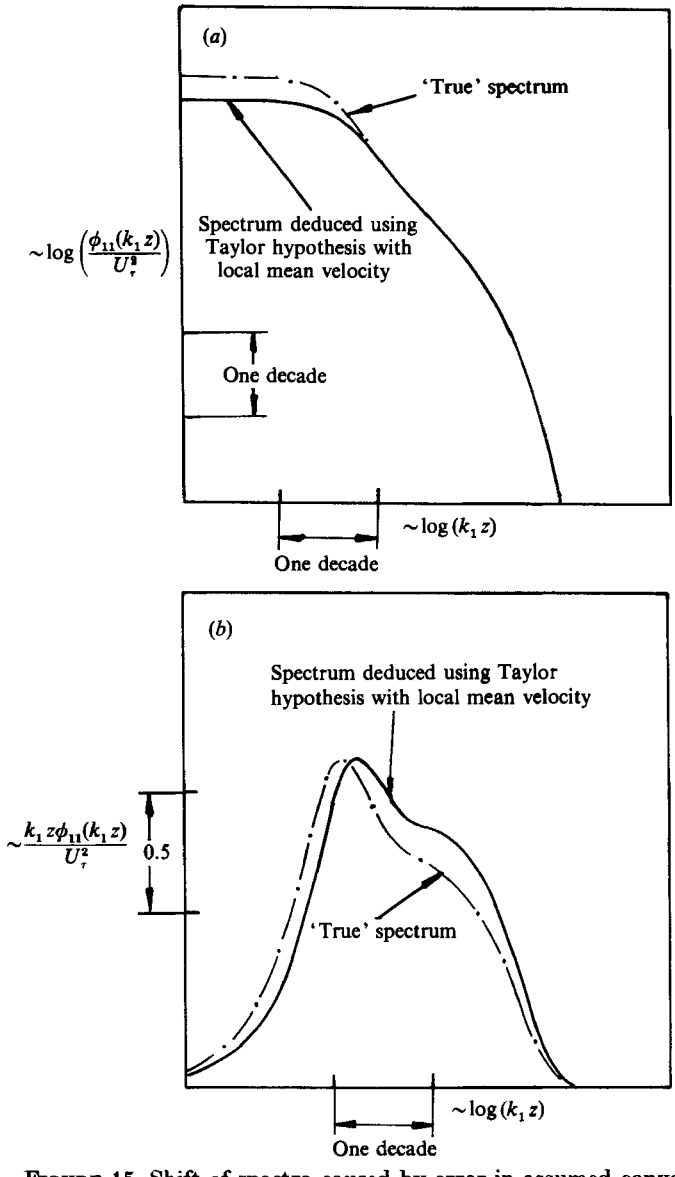

FIGURE 15. Shift of spectra caused by error in assumed convection velocity.

velocity of the observer. By using the Reynolds-number similarity argument, they showed that for certain regions of (k_1, c)-space for a given z/δ_H

$$\frac{W}{z^2 U_\tau} = q\left(k_1 z, \frac{c-U}{U_\tau}\right). \tag{28}$$

Assuming that the small-scale motions are convected at the local mean velocity U while the large-scale motions are convected at a velocity close to U_1, a fractional spread of order $(U_1 - U)/U_1$ in convection velocity would exist. It can be seen that the larger the U_1/U_τ is, the smaller the fractional spread in convection velocities $(U_1 - c)/U_1$.

Figure 16 shows schematically how an error is involved when transforming the spectrum from the frequency domain to the wavenumber domain. The figure shows

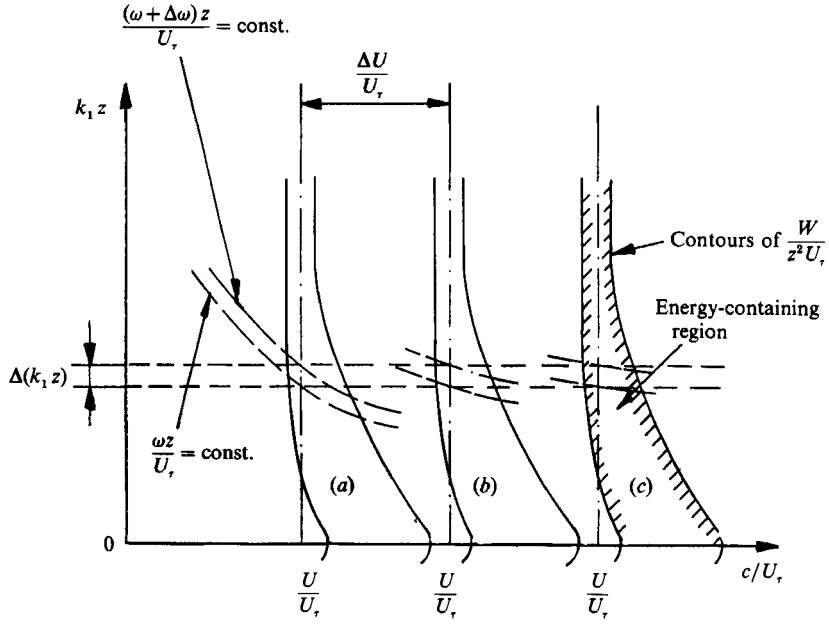

FIGURE 16. Conjecture contours of the spectral function W/z^2U_τ: (*a*) rough-wall case; (*b*) smooth-wall case, same Reynolds number; (*c*) smooth-wall case, high Reynolds number. (After Perry & Abell.)

the same $W(k, c)$ contours at three different U_1/U_τ values. One is for the low-Reynolds-number smooth-wall case, another for a rough wall and the third is for smooth wall at very high Reynolds number. The spectrum $\phi_{11}(k_1 z)/U_\tau^2$ is obtained by integrating $W(k_1 z, c/U_\tau)/z^2U_\tau$ along horizontal strips $\Delta(k_1 z)$ wide. However, in the frequency domain, this integration is along $\Delta(\omega z/U_\tau)$ which are hyperbolic strips shown in the figure, where ω is the circular frequency. It can be seen that the smaller the U_1/U_τ is, the larger the error involved in the inferred spectrum. On low-Reynolds-number rough walls this effect would be very serious, while at very high Reynolds numbers the fractional spread in convection velocity diminishes and Taylor's hypothesis can be used safely as $U_1/U_\tau \to \infty$.

Experimentally, we would prefer to move a probe so rapidly through the turbulence that the velocity field does not change appreciably during the time of measurement. As suggested by Tennekes & Lumley (1972, p. 253), if the traversing speed q of the probe is large enough, the velocity signal $u_1(t)$ may be identified with $u_1(x/q)$. Although we do not normally move the probe through the flow to obtain the spectrum, the 'flying' hot-wire system gives us a unique opportunity to investigate the effects of this convection velocity spread and check the above conjectures. This is possible in spite of the fact that the velocity of the probe is limited to 3.5 m/s in the upstream direction. Of course the present flying hot wire will not resolve the convection velocity problem since it is not flying at a speed large compared with the spread in convection velocity.

Figures 17 and 18 show the two streamwise spectra measured over the smooth and the *k*-type rough walls by using the flying and stationary hot wires. Both figures show clearly the effect of this spread in convection velocity and agree with the crude simulation results as shown in figure 15(*a*, *b*). Comparing figure 17 with figure 18, it can be seen that this spread in convection velocity on rough walls is more pronounced and is consistent with the conjecture mentioned above.

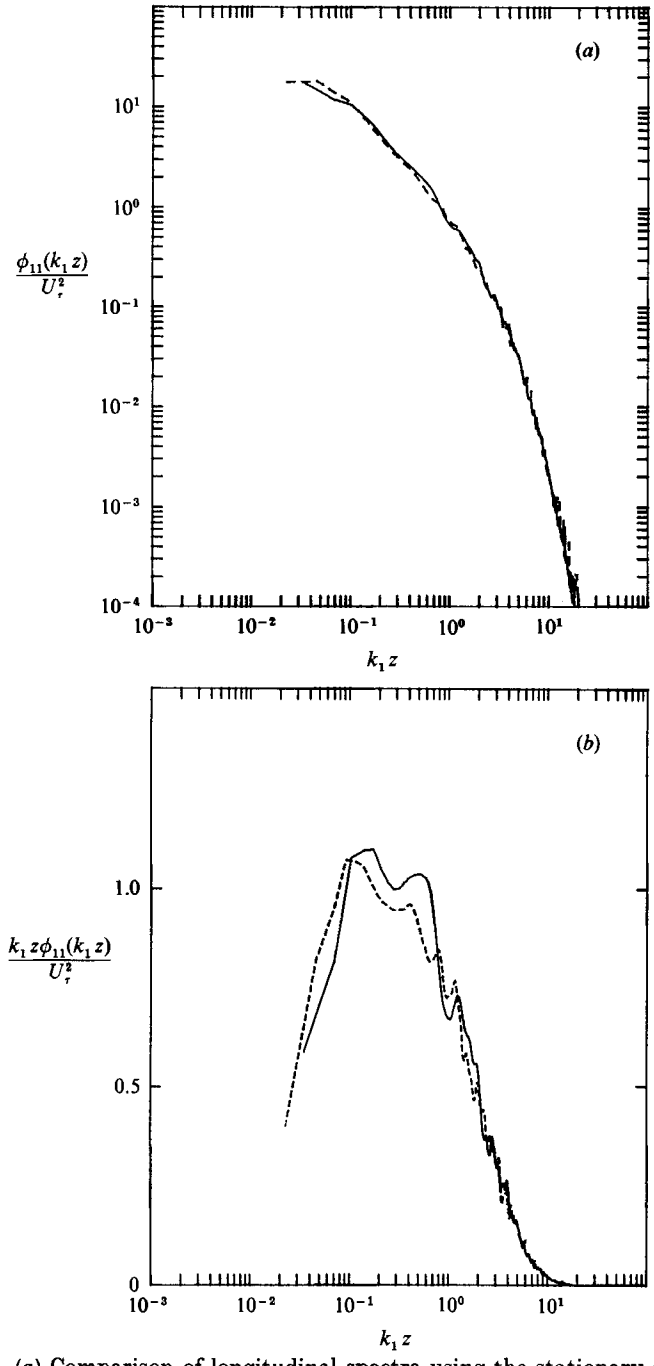

FIGURE 17. (*a*) Comparison of longitudinal spectra using the stationary and flying wires, smooth wall. (*b*) Comparison of pre-multiplied longitudinal spectra using the stationary and flying wires, smooth wall. ——, Stationary hot wire; – – – –, flying hot wire; Sled velocity = 3.5 m/s; U_1 = 10 m/s, $z/\delta_H = 0.12$.

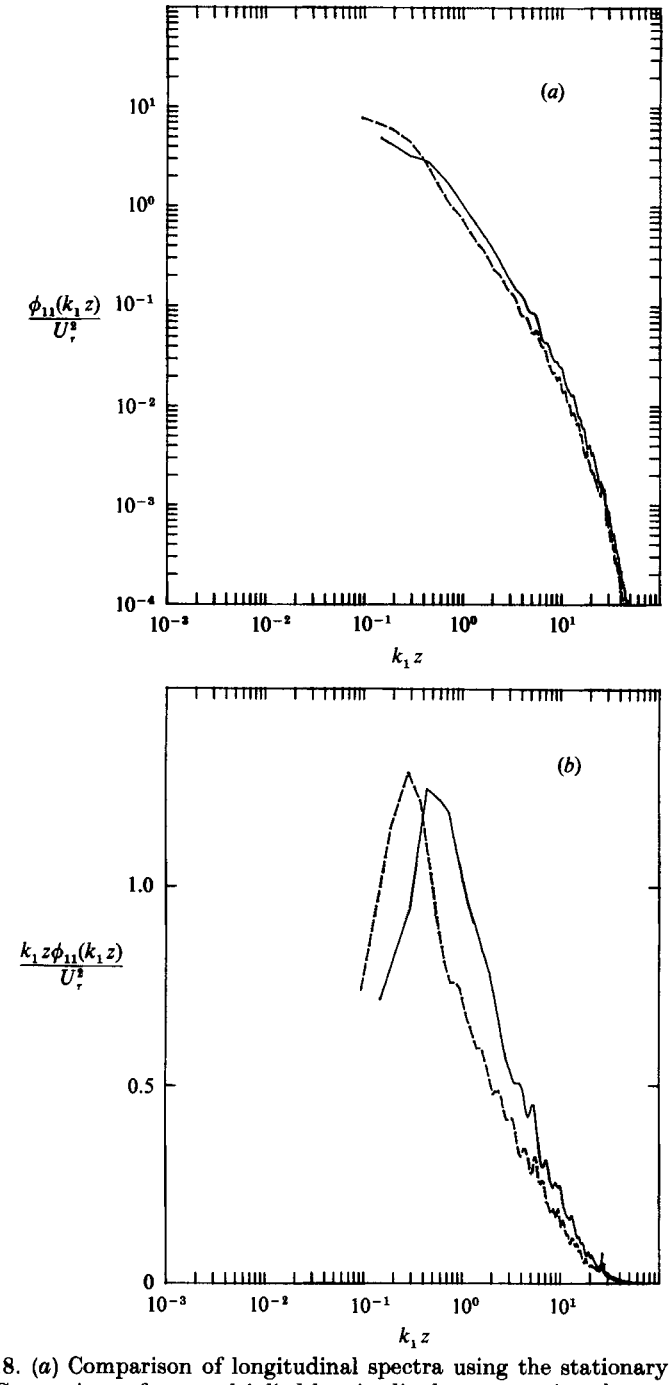

FIGURE 18. (*a*) Comparison of longitudinal spectra using the stationary and flying wires, rough wall. (*b*) Comparison of pre-multiplied longitudinal spectra using the stationary and flying wires, rough wall. Symbols and conditions as figure 17.

Using the attached-eddy hypothesis and the Perry & Chong (1982) model, it is known that for the motions normal to the wall, most of the energy comes from the eddies that scale with the distance from the wall. Because these eddies are probably being convected downstream at close to the local mean velocity, when transforming the spectrum from the frequency domain to the wavenumber domain using the local mean velocity, the spread in convection velocity for the component normal to the wall would be smaller than that for the streamwise component. This has been checked by measuring the normal-component spectra over the smooth and k-type rough walls using the flying and stationary hot wires. Figures 19 and 20 show these results and it can be seen that this convection velocity effect is small for this component, as conjectured using the Perry *et al.* model (1986).

5.2. *Streamwise turbulence spectra in the turbulent wake region*

Figure 21 shows the spectra measured from $z/\delta_H = 0.0302$ to 1.0225 at $K_\tau = 4433$ over the smooth wall. The figure shows that from $z/\delta_H = 0.7$ and beyond, the spectra do not collapse with the spectra at $z/\delta_H < 0.7$ in any wavenumber region. The results contrast with those measured in pipe flow (Perry *et al.* 1986), where it is found that the spectra measured in the central part of the pipe flow collapse with those near the wall at high wavenumber. The reason for this difference might be because of the intermittent nature of the outer part of the layer. Because of this intermittency effect, the measured broadband turbulence intensity will be less than that measured in a pipe flow at the same corresponding position where the intermittent factor equals one, i.e. where the flow is fully turbulent. After normalization with the broadband turbulence intensity, the spectrum in the outer region of the turbulent boundary layer will be shifted down compared with that in a pipe flow

At very low wavenumber, each spectrum shows a gradual rise as $k_1 \rightarrow 0$ starting from $z/\delta_H = 0.5$. This rise becomes larger as we move away from the wall and is thought to be due to the free-stream turbulence effect and possibly low-frequency unsteadiness of the wind tunnel as well as the irrotational flow induced by the turbulent flow in the boundary layer.

One important characteristic of spectra in the outer region is that they show an obvious $-\frac{5}{3}$ power-law region and its extent increases as z/δ_H increases. For the spectra measured within $0.7 < z/\delta_H < 1$, although they do not collapse with each other when plotted as in figure 21, the spectra clearly follow the $-\frac{5}{3}$ power law in the high-wavenumber region.

5.3. *Spanwise- and normal-component spectra in the turbulent wall region*

Figures 22, 23 and 24 show ϕ_{22} plotted with inner-flow, Kolmogorov and outer-flow scalings respectively. Only smooth-wall results were measured. Figure 25 and 26 show the spectra normal to the wall with inner and Kolmogorov scaling for both smooth and k-type roughness. The data and scaling are much the same as in Perry *et al.* (1987).

Two important points about ϕ_{33} results, which the authors recently realized, concern the lack of collapse of ϕ_{33} at low wavenumbers with inner-flow scaling as shown in figure 25. The stationary and flying-hot-wire results in figure 19 and 20 show that this spread is not due to a convection velocity effect. According to the Biot–Savart law calculations for the attached-eddy simulation of wall turbulence of Perry *et al.* (1986) (their figure 25*b*) low-wavenumber collapse occurs only for $z/\delta_H < 0.03$. The lowest value of z/δ_H reported here was $z/\delta_H > 0.03$. If the wall region is defined to be $z_+ > 100$ and $z/\delta_H < 0.15$ as in Perry *et al.* (1987) (which is

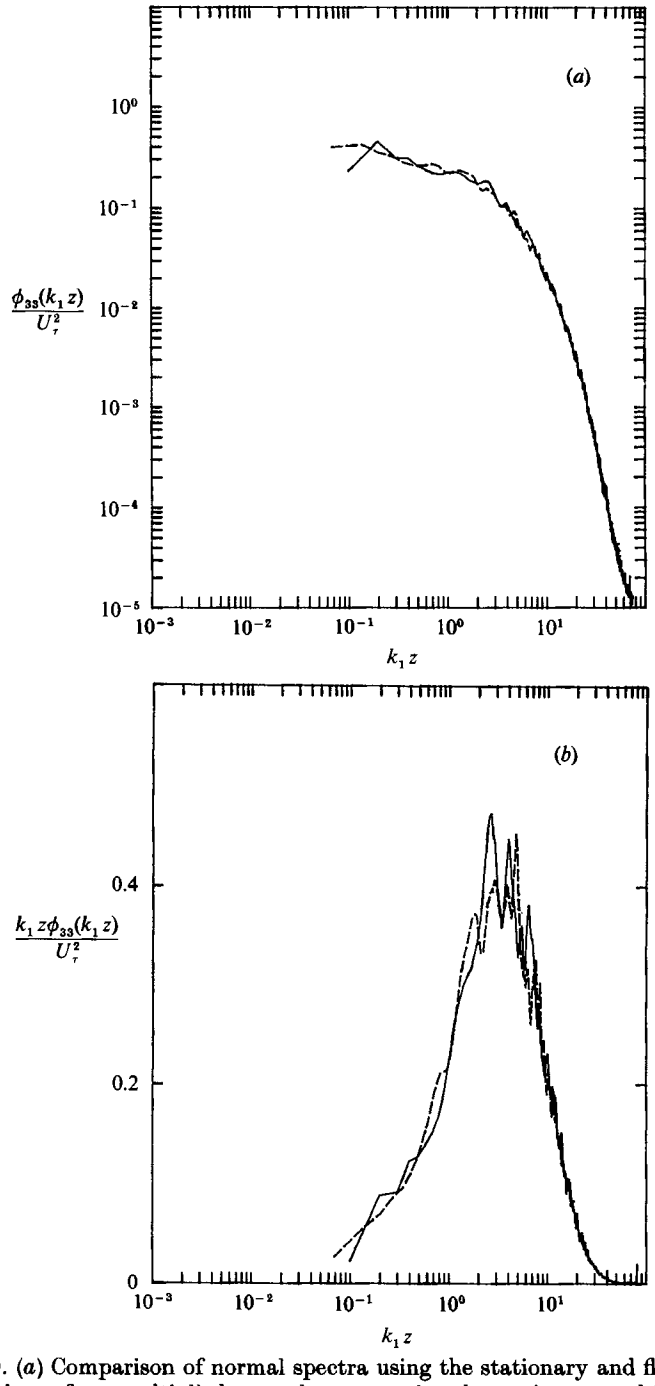

FIGURE 19. (*a*) Comparison of normal spectra using the stationary and flying wires, smooth wall. (*b*) Comparison of pre-multiplied normal spectra using the stationary and flying wires, smooth wall. Symbols and conditions as figure 17.

somewhat liberal), then the computations show that a spread of one octave in $\phi_{33}(k_1 z)/U_\tau^2$ is possible and this is close to the low-wavenumber spread seen in figure 25. Another problem which could affect the collapse is an electronic mismatch of the $\times$-wires used. Figure 12 shows that at the same low wavenumbers $\phi_{11}(k_1 z)/U_\tau^2$ is of

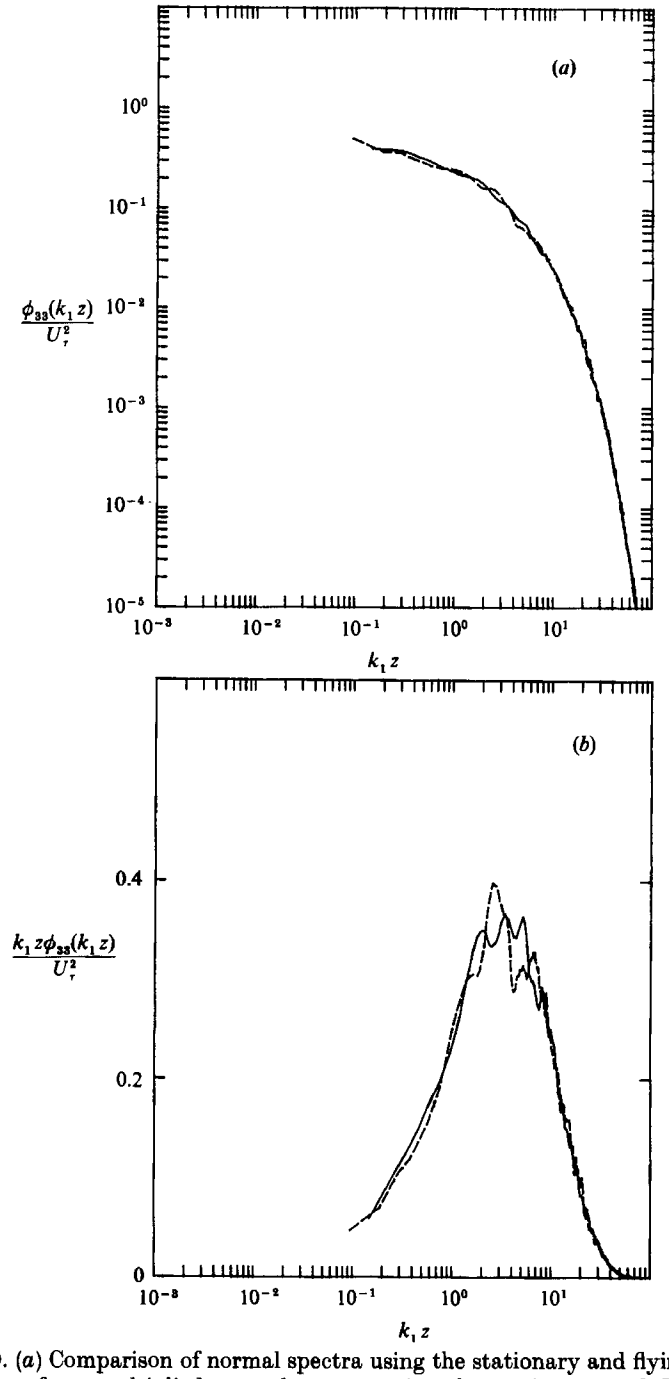

FIGURE 20. (*a*) Comparison of normal spectra using the stationary and flying wires, rough wall. (*b*) Comparison of pre-multiplied normal spectra using the stationary and flying wires, rough wall. Symbols and conditions as figure 17.

order 40 while figure 25 shows that $\phi_{33}(k_1 z)/U_\tau^2$ is of order 1. Thus a slight mismatch of the $\times$-wires will cause a u_1 component contamination and this will affect the $\phi_{33}(k_1 z)/U_\tau^2$ values significantly at low wavenumbers.

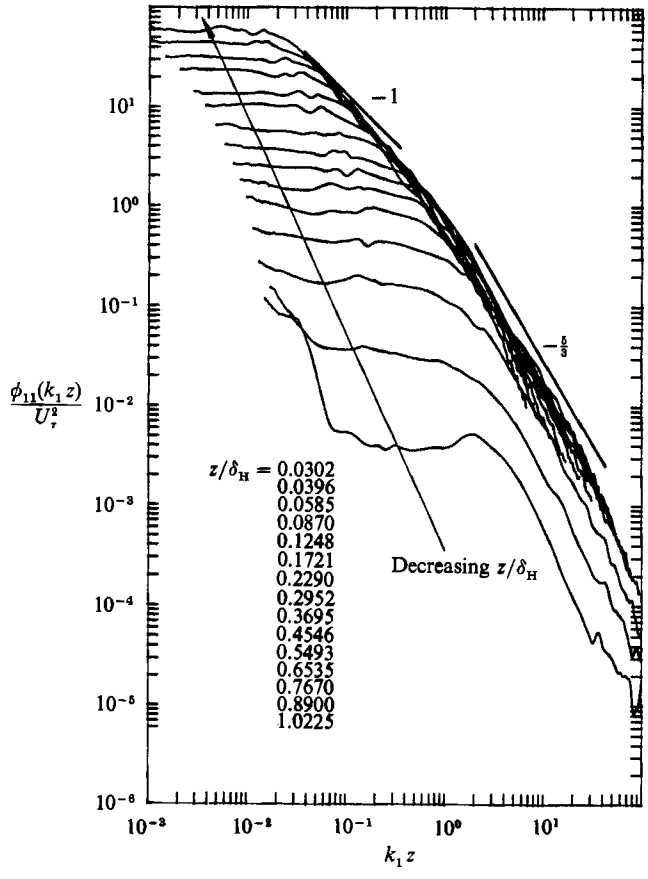

FIGURE 21. Longitudinal spectra in the whole fully turbulent region at $K_\tau = 4433$, smooth wall.

6. Conclusions and discussion

This work provides further support of the Townsend (1976) attached-eddy hypothesis and the various models based on this as put forward by Perry & Abell (1977), Perry & Chong (1982) and Perry *et al.* (1986, 1987). The broadband turbulence intensity distributions are Reynolds-number invariant for most of the flow except in the turbulent wall region where a viscous correction term $V(z_+)$ needs to be applied. This quantity, which represents the energy missing because of the viscous dissipation range, can be derived from the classical Kolmogorov theory of local isotropy. Although doubts may be raised about the validity of this theory in the turbulent wall region for the relatively low Reynolds numbers encountered in the laboratory, it certainly is consistent with the size of the Reynolds-number effect observed.

Three levels of approximation have so far been formulated for determining $V(z_+)$. Perry & Abell (1977) gave $V(z_+) = C(z_+)^{-\frac{1}{2}}$ for the u_1 component and this was extended by Perry *et al.* (1986) to $V(z_+) = \frac{4}{3}C(z_+)^{-\frac{1}{2}}$ for the u_2 and u_3 components. This assumed a sudden cutoff of energy from the $-\frac{5}{3}$ law at a scale proportional to the Kolmogorov scale. It has been shown that this result is too crude: the $\frac{4}{3}$ factor is due to a mathematical oversight and its inclusion violates the condition of isotropy. Better approximations to $V(z_+)$ have been derived here using the Kovasznay *spectral* formula and, as Spalart (1988) pointed out, $V(z_+)$ should be isotropic, i.e. the same for all three components. Equation (17) is based on this and has the advantage of

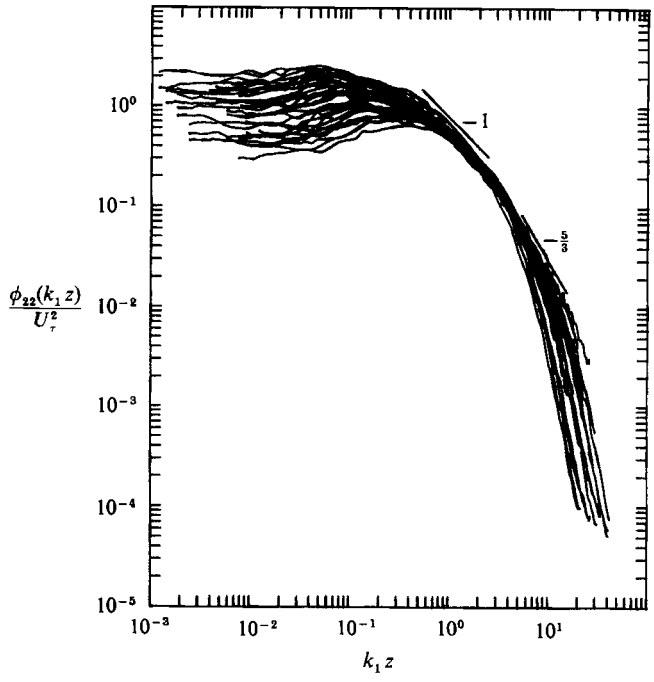

FIGURE 22. Spanwise spectra in the turbulent wall region, inner-flow scaling: $z/\delta_H < 0.15$, $zU_\tau/\nu > 100$.

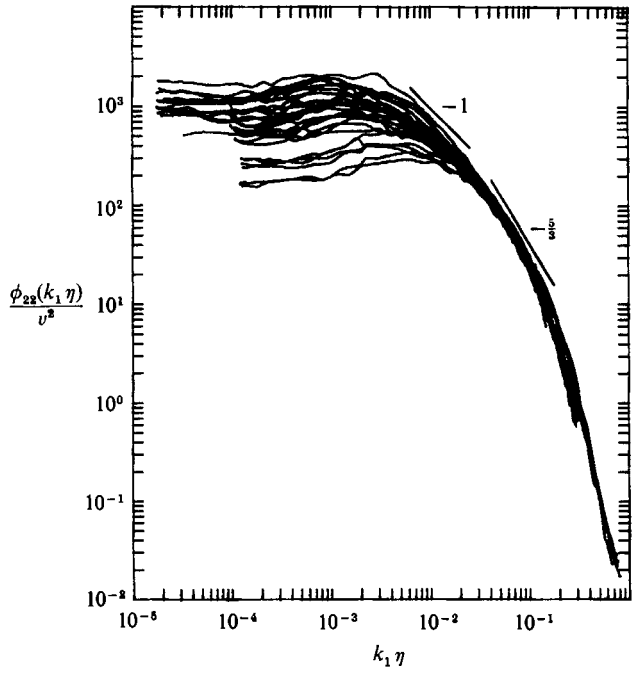

FIGURE 23. Spanwise spectra in the turbulent wall region, Kolmogorov scaling: $z/\delta_H < 0.15$, $zU_\tau/\nu > 100$.

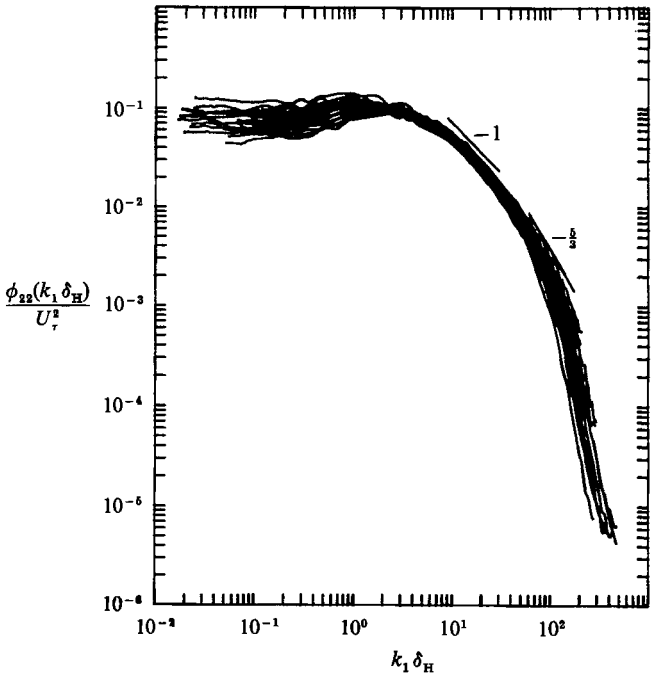

FIGURE 24. Spanwise spectra in the turbulent wall region, outer-flow scaling: $z/\delta_H < 0.15$, $zU_\tau/\nu > 100$.

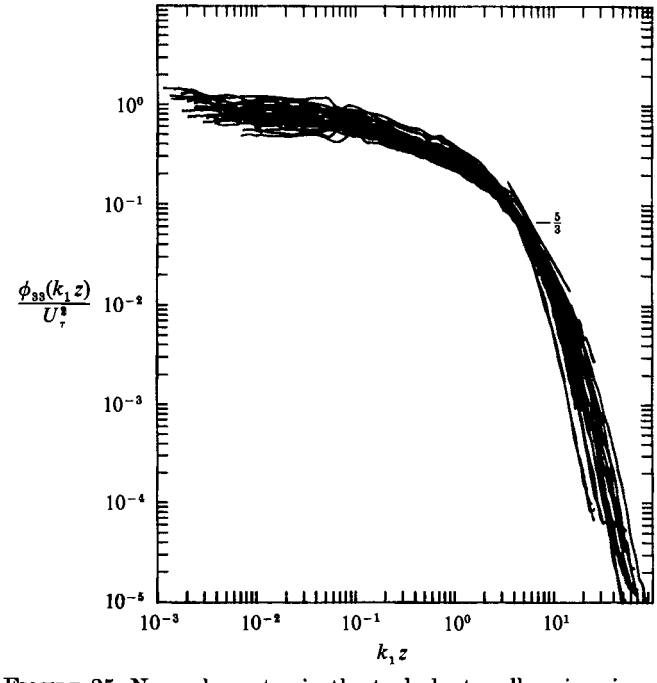

FIGURE 25. Normal spectra in the turbulent wall region, inner-flow scaling: $z/\delta_H < 0.15$, $zU_\tau/\nu > 100$.

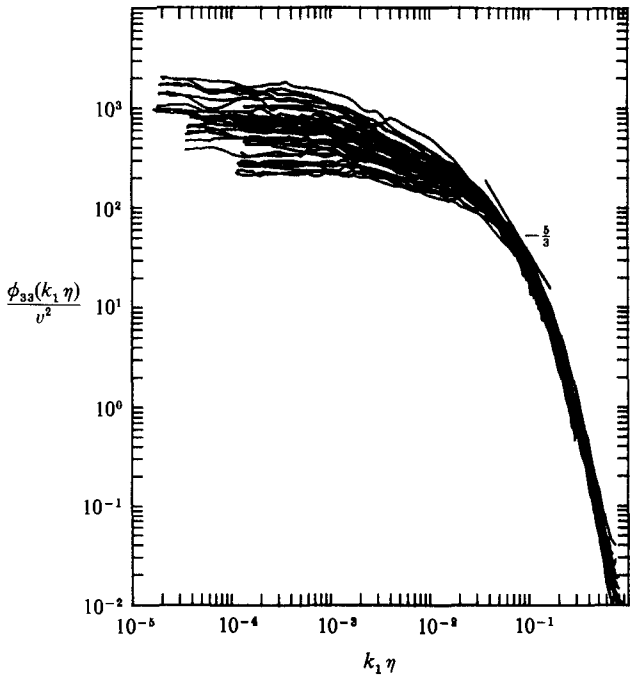

FIGURE 26. Normal spectra in the turbulent wall region, Kolmogorov scaling: $z/\delta_H < 0.15$, $zU_\tau/\nu > 100$.

giving an analytical expression which fits the data well except at low z_+. However, a more logical formulation is given by (21) and this fits the data best over the whole range of z_+. But this formulation can only be used numerically and there is still a degree of arbitrariness contained in it.

The quantity $\overline{u_3^2}/U_\tau^2$ is very difficult to measure accurately. However, by considering only the data where it was possible to estimate the spatial resolution effect and avoiding cases where cone angles may have been a problem or where there were anomalies in the $-\overline{u_1 u_3}/U_\tau^2$ distributions, very encouraging correlations were found. The authors have successfully correlated quite a broad range of data from disparate flow cases from a number of workers by using (21) and (25), as seen in figure 11. Smooth-wall results, *k*-type and *d*-type roughness results, subminature probe results, flying-hot-wire results and the computer simulation results of Spalart all fall close to the one universal curve.

The inconsistency of the various universal constants given in Perry *et al.* (1987) for smooth and rough walls for all three components have been removed and spatial resolution corrections played a significant part in this.

The convection velocity problem, anticipated many years ago, for example Wills (1964) and Perry & Abell (1977), has been verified for wall turbulence by the use of the flying hot wire. The lack of collapse at low wavenumbers of the streamwise spectra with outer-flow scaling is explained in terms of this convection velocity problem. The fact that the spectra of the component normal to the wall are unaffected by the velocity of the probe when using Taylor's-hypothesis transformation for converting frequency to wavenumber adds further support to the attached-eddy hypothesis since this is consistent with most of the energy being derived from one hierarchy scale or at least a narrow band of scales, whereas for the streamwise and spanwise components a broad range of hierarchy scales are involved.

The lack of collapse at the low wavenumbers for the normal-component spectra when expressed with inner-flow scaling may be due to a too liberal definition being used for the turbulent wall region. Also cross-contamination of the u_3 velocity signature with u_1 fluctuations may cause problems at very low wavenumbers.

The authors wish to thank Dr S. M. Henbest for his help in this project. We would also like to thank the Australian Research Grants Committee and Australian Research Council for their financial support.

Appendix

Throughout this paper, the boundary-layer thickness δ_H is defined using the Coles' (1956, 1962) law of the wall and law of the wake.

$$\frac{U}{U_\tau} = \frac{1}{\kappa}\ln\frac{zU_\tau}{\nu} + A - \frac{\Delta U}{U_\tau} + \frac{\Pi}{k}\xi\left(\frac{z}{\delta_c}\right), \tag{A 1}$$

where δ_c is Coles' boundary-layer thickness and it is the value of z where the velocity profile has a maximum departure from the logarithmic law. A modification to (A 1) with the suggested wake function given by Hinze (1959) is given in Li (1989) and Li & Perry (1989) as

$$\frac{U}{U_\tau} = \frac{1}{\kappa}\ln\frac{zU_\tau}{\nu} + A - \frac{\Delta U}{U_\tau} + \frac{\Pi}{\kappa}\left(1-\cos\left(\beta\pi\frac{z}{\delta_H}\right)\right), \tag{A 2}$$

and the factor β is found from

$$1 + \beta\pi\Pi\sin(\beta\pi) = 0. \tag{A 3}$$

This ensures that the velocity profile has zero slope at the outer edge.

The defect law based on (A 2) is

$$f(\eta) = \frac{U_1 - U}{U_\tau} = -\ln\eta + \frac{\Pi}{\kappa}(-\cos(\beta\pi) - \cos(\beta\pi\eta)), \tag{A 4}$$

where $\eta = z/\delta_H$.

The boundary-layer thickness was calculated using the integration method

$$\delta_H = \frac{\delta^* U_1}{C_1 U_\tau}, \tag{A 5}$$

where δ^* is the displacement thickness, $C_1 = \int_0^1 f\,\mathrm{d}\eta$ and C_1 is a known function of Π. In zero-pressure-gradient turbulent boundary layers, Π varies slightly from station to station. This was taken into account in calculating C_1 whereas Perry *et al.* (1987) assumed C_1 to be constant. The ratio of δ_{99} to δ_H is dependent on U_1/U_τ. For a typical value of $U_1/U_\tau = 27$, $\delta_{99}/\delta_H \approx 0.83$ and $\delta_{995}/\delta_H \approx 0.89$.

REFERENCES

BANDYOPADHYAY, P. R. 1987 *J. Fluid Mech.* **180**, 231–266.

BATCHELOR, G. K. 1953 *The Theory of Homogeneous Turbulence.* Cambridge University Press.

BREMHORST, K. 1972 *Trans. IEEE Instrum Meas.* IM **21**, 244–248.

CLAUSER, F. H. 1954 *J. Aero. Sci.* **21**, 91–107.

COLES, D. 1956 *J. Fluid Mech.* **1**, 191–226.

COLES, D. 1962 *USAF. The Rand Cooperation*, Rep. R-403-PR, Appendix A.

ERM, L. P., SMITH, A. J. & JOUBERT, P. N. 1986 *Turbulent Shear Flows 5* (ed. F. Durst, B. E. Launder, J. L. Lumley, F. W. Schmidt & J. H. Whitelaw). Springer.

HAMA, F. R. 1954 *Soc. Naval Archit. Marine Engng, New York, Paper* 6.

HINZE, J. O. 1975 *Turbulence*, 2nd edn. McGraw-Hill.

KOLMOGOROV, A. N. 1941 *C.R. Acad. Sci. USSR* **30**, 301.

KOVASZNAY, L. S. G. 1948 *J. Aero. Sci.* **15**, 745–753.

LI, J. D. 1989 The turbulence structure of wall shear flow. Ph.D. thesis, University of Melbourne, Australia.

LI, J. D., HENBEST, S. M. & PERRY, A. E. 1986 *Proc. 9th Australasian Fluid Mech. Conf., Auckland.*

LI, J. D. & PERRY, A. E. 1989 *Proc. 10th Australasian Fluid Mech. Conf., Melbourne.*

LIGRANI, P. M. & BRADSHAW, P. 1987 *J. Phys.* E: Sci. Instrum. **20**, 323–332.

LIGRANI, P. M. & BRADSHAW, P. 1987 *Expts. Fluids* **5**, 407–417.

LIGRANI, P. M., WESTPHAL, R. V. & LEMOS, F. R. 1989 *J. Phys* E: *Sci. Instrum.* **22**, 262–268.

LIM, K. L. 1985 Wall shear flow. Ph.D. thesis, University of Melbourne, Australia.

LIN, C. C. 1952 *Q. Appl. Maths* **10**, 295.

NAKAYAMA, A. & WESTPHAL, R. V. 1986 *NASA TM*-883522.

PAO, Y. H. 1965 *Phys. Fluids* **8**, 1063–1108.

PATAL, V. C. 1965 *J. Fluid Mech.* **23**, 185–208.

PERRY, A. E. 1982 *Hot-Wire Anemometry*. Clarendon.

PERRY, A. E. 1987 *Perspective in Turbulence Studies* (ed. H. U. Meier & P. Bradshaw), pp. 115–153. Springer.

PERRY, A. E. & ABELL, C. J. 1967 *J. Fluid Mech.* **79**, 785–799.

PERRY, A. E. & CHONG, M. S. 1982 *J. Fluid Mech.* **119**, 173–217.

PERRY, A. E., HENBEST, S. M. & CHONG, M. S. 1986 *J. Fluid Mech.* **165**, 163–199.

PERRY, A. E. & JOUBERT, P. N. 1963 *J. Fluid Mech.* **17**, 193–211.

PERRY, A. E., LI, J. D., HENBEST, S. M. & MARUŠIĆ, I. 1988*a* *Zoran Zaric Memorial Intl Sem. on Near Wall Turbulence, Dubrovnik*. Hemisphere (to appear).

PERRY, A. E., LI, J. D. & MARUŠIĆ, I. 1988*b* *AIAA*-88-0219.

PERRY, A. E., LIM, K. L., HENBEST, S. M. & CHONG, M. S. 1983 *Proc. 4th Intl Symp. on Turbulent Shear Flow, Karlsruhe*, pp. 113–117.

PERRY, A. E., LIM, K. L. & HENBEST, S. M. 1987 *J. Fluid Mech.* **177**, 437–466.

PERRY, A. E., SCHOFIELD, W. H. & JOUBERT, P. N. 1969 *J. Fluid Mech.* **37**, 383–413.

PERRY, A. E., SMITS, A. J. & CHONG, M. S. 1979 *J. Fluid Mech.* **90**, 415–431.

ROBERTS, J. B. 1973 *Aero. J.* **77**, 406–412.

SPALART, P. R. 1988 *J. Fluid Mech.* **187**, 61–98.

TANI, I. 1987 *Perspective in Turbulence Studies* (ed. H. U. Meier & P. Bradshaw), pp. 223–249. Springer.

TAYLOR, G. I. 1938 *Proc. R. Soc. Lond.* A **164**, 476–490.

TENNEKES, H. & LUMLEY, J. L. 1972 *A First Course in Turbulence*. M.I.T. Press.

TOWNSEND, A. A. 1976 *The Structure of Turbulent Shear Flow*, 2nd edn. Cambridge University Press.

UBEROI, M. S. & KOVAZSZAY, L. S. G. 1953 *Q. Appl. Maths* **10**, 375–393.

WEI, T. & WILLMARTH, W. W. 1989 *J. Fluid Mech.* **204**, 57–95.

WILLMARTH, W. W. & BOGAR, T. J. 1977 *Phys. Fluids* **20**, S9–S21.

WILLMARTH, W. W. & SHARMA, L. K. 1984 *J. Fluid Mech.* **142**, 121–149.

WILLS, J. A. B. 1964 *J. Fluid Mech.* **20**, 417–432.

WYNGAARD, J. C. 1968 *J. Sci. Instrum.* (2) **1**, 1105–1108.

ZAMAN, K. B. M. Q. & HUSSAIN, A. K. M. F. 1981 *J. Fluid Mech.* **112**, 379–396.